Report to:

National Earthquake Hazards Reduction Program,
External Research Program
Reston, VA

Award Number 07HQGR0112

Volume Change in Unsaturated Soils from Cyclic Loading

by

Jonathan P. Stewart (PI)
Eric Yee and Pendo Duku (Graduate Students)

University of California, Los Angeles
Civil & Environmental Engineering Department

May, 2009

ACKNOWLEDGEMENTS

Support for this work was provided by the U.S. Geological Survey (USGS), Department of the Interior, under USGS award No. 07HQGR0112. The views and conclusions contained in this document are those of the authors and should not be interpreted as necessarily representing the official policies, either expressed or implied, of the U.S. Government.

ABSTRACT

USGS/NEHRP Award No. 07HQGR0112

VOLUME CHANGE IN UNSATURATED SOILS FROM CYCLIC LOADING

PI: Jonathan P. Stewart
Civil & Environmental Engineering Department
University of California
Los Angeles, CA 90095-1593
Tel: (310) 206 2990 Fax: (310) 206 2222
jstewart@seas.ucla.edu

Seismic compression is the accumulation of contractive volumetric strains in unsaturated soil from earthquake shaking. This type of ground deformation is a significant and costly earthquake hazard that has been documented in numerous prior seismic events (Pyke et al. 1975, Stewart et al. 2001, 2004, Wartman et al. 2003, Tokimatsu 2008).

Initial laboratory investigations of seismic compression focused on clean sands (Silver and Seed 1971, Youd 1972, Pyke et al. 1975, Duku et al., 2008). These tests showed that relative density, overburden stress, stress history, and various demand parameters (cyclic shear strain amplitude, number of shear strain cycles, and multi-directional shaking) significantly influence vertical strain. Duku et al. (2008) synthesized these results into a volumetric strain material model (VSMM) for clean sands, which relates the shear strain demand applied to a soil element to the resulting volume change. VSMMs can be used with shear strains estimated from site response analysis to estimate the settlements from seismic compression.

Seismic compression of soils with fines has been investigated by Whang et al (2004, 2005), who conducted simple shear testing on sands with varying fines content of varying plasticity. They found vertical strains to be influenced by relative compaction,

intermediate saturation levels, and fines content under a constant relative compaction. DC-SS testing by Duku et al. (2006) showed the influence of ageing effects on plastic soils. The principal thrust of the present investigation was to further advance our understanding of overburden and stress history effects on fine-grained soils. An additional task we found to be necessary to characterize small-strain behavior was the development of improved data processing procedures that formally quantify the uncertainty in data points given noise in the data acquisition system.

Digitally-controlled simple shear (DC-SS) testing was performed on a sand material mixed with various amounts of low-plasticity fines. The results show vertical strain at fifteen shear strain cycles increases as relative density, overburden pressure, and OCR decrease, which is similar to previous test results on clean sands (Duku et al. 2008). These tests also showed an increase in vertical strain for increasing fines content, contradicting previous research by Whang et al. (2004) who found seismic compression susceptibility of a similar material to be lower than typical clean sand materials. We now understand that the particular soil tested in the present investigation and by Whang et al. (2004) exhibits seismic compression behavior that is lower than average. Accordingly, the Whang et al (2004) results are not in conflict with the present findings.

Statistical techniques were compared in evaluating the variability of horizontal displacement measurements of the DC-SS device. These techniques involve the confidence intervals on the displacement amplitude from spectral analysis and linear regression of a transformed variable. After comparing these methods, the recommended procedure for evaluating horizontal displacement amplitude is through spectral analysis. Confidence intervals for the vertical displacements were produced using kernel smoothing with the Nadaraya-Watson estimator and a Gaussian kernel. The results of kernel smoothing and the noise profile were compared to provide a more robust estimate of volumetric threshold shear strain than has previously been possible.

TABLE OF CONTENTS

1. INTRODUCTION 1
   1.1 SEISMIC COMPRESSION 1
   1.2 LITERATURE REVIEW 1
      1.2.1 CASE HISTORIES 1
      1.2.2 PREVIOUS RESEARCH IN SEISMIC COMPRESSION OF CLEAN SANDS 6
      1.2.3 PREVIOUS RESEARCH IN SEISMIC COMPRESSION OF SANDS WITH FINES 10
   1.3 PRESENT STUDY 12
2. DATA ANALYSIS 13
   2.1 UCLA DIGITALLY CONTROLLED SIMPLE SHEAR DEVICE 13
   2.2 CYCLIC SHEAR STRAIN VARIABILITY 14
      2.2.1 NOISE FROM HORIZONTAL MEASUREMENTS WITH ZERO COMMAND SIGNAL 15
      2.2.2 QUANTIFICATION OF HORIZONTAL MEASUREMENT VARIATION 17
         2.2.2.1 SPECTRAL ANALYSIS 17
         2.2.2.2 REGRESSION 19
      2.2.3 RESULTS OF HORIZONTAL MEASUREMENT ANALYSIS 20
   2.3 VERTICAL STRAIN VARIABILITY 22
      2.3.1 NOISE FROM VERTICAL MEASUREMENTS 22
      2.3.2 QUANTIFICATION OF VERTICAL MEASUREMENT VARIATION 24
      2.3.3 RESULTS OF VERTICAL MEASUREMENT ANALYSIS 27
      2.3.4 UTILIZATION OF VERTICAL DISPLACEMENT ERROR MEASUREMENT TO EVALUATE DISPLACEMENTS AT THE VOLUMETRIC THRESHOLD SHEAR STRAIN 29
3. SEISMIC COMPRESSION BEHAVIOR OF A SAND-FINES MIXTURE INCLUDING OVERBURDEN AND STRESS HISTOY EFFECTS 32
   3.1 SOIL TESTED 32
   3.2 LABORATORY TEST EQUIPMENT AND PROTOCOLS 33
   3.3 RESULTS OF CYCLIC SIMPLE SHEAR TESTS 33
      3.3.1 FORM AND PARAMETERIZATION OF RESULTS 33
      3.3.2 EFFECT OF RELATIVE DENSITY AND FINES CONTENT 34
         3.3.2.1 EFFECT OF RELATIVE DENSITY AND FINES CONTENT ON VERTICAL STRAIN 34
         3.3.2.2 EFFECT OF RELATIVE DENSITY AND FINES CONTENT ON NORMALIZED VERTICAL STRAIN 39
      3.3.3 EFFECT OF OVERBURDEN 41
         3.3.3.1 EFFECT OF OVERBURDEN ON VERTICAL STRAIN 41
         3.3.3.2 EFFECT OF OVERBURDEN ON NORMALIZED VERTICAL STRAIN 43
      3.3.4 EFFECT OF OCR 44
         3.3.4.1 EFFECT OF OCR ON VERTICAL STRAIN 44
         3.3.4.2 EFFECT OF OCR ON NORMALIZED VERTICAL STRAIN 46
      3.3.5 EFFECT OF PRIOR CYCLIC LOADING 47

4. SUMMARY AND FUTURE RESEARCH NEEDS 49

TABLE OF FIGURES

Figure 1.1 – Jensen Filtration Plant profile (Pyke et al. 1975). 2
Figure 1.2 – Plan and settlement of Site B (Stewart et al. 2004)..... 4
Figure 1.3 – Aerial photograph of Kashiwazaki-Kariwa nuclear power plant (Tokimatsu 2008). 5
Figure 1.4 – Cross sections of Kashiwazaki-Kariwa nuclear power plant (Tokimatsu 2008). 6
Figure 1.5 – Effect of surcharge on vertical strain (Silver and Seed 1971)..... 7
Figure 1.6 – Effect of surcharge on vertical strain (Silver and Seed 1971)..... 8
Figure 1.7 – Comparison of settlements under (a) components and combined random motions and (b) in three-dimensional shake table tests (Pyke et al. 1975)..... 8
Figure 1.8 – Simplified procedure for dry sands: (a) relationship between volumetric strain, shear strain, and penetration resistance and (b) relationship between volumetric strain ratio and number of cycles (Tokimatsu and Seed 1987)..... 9
Figure 1.9 – Comparison of cyclic vertical strain behavior for fill soils with low-plasticity fines and clean sands (Whang et al 2004). 10
Figure 1.10 – Fines content and saturation effects on seismic compression behavior (Whang et al. 2005)..... 11
Figure 2.1 – Photographs of UCLA DC-SS showing (a) overview, (b) view of frame and adapter plate, and (c) soil sample in wire-reinforced membrane between caps (Duku et al. 2007)..... 13
Figure 2.2 – Normalized root mean square of tracking errors for (a) unidirectional and (b) multidirectional broadband command signals of different amplitude (Duku et al. 2007). 14
Figure 2.3 – Sample sinusoidal wave command and corresponding feedback..... 15
Figure 2.4 – Sample noise feedback signal from horizontal LVDT for (a) trial 1 and (b) trial 2. 16
Figure 2.5 – Distribution of sample noise feedback signal and normal probability distribution fit to the data for (a) trial 1 and (b) trial 2. 16
Figure 2.6 – Frequency domain representation of sample feedback and command signal. 19
Figure 2.7 – Error metrics from sample tests for (a) normalized root mean square error and (b) 95% confidence interval range..... 21
Figure 2.8 – Sample vertical displacement output. 22
Figure 2.9 – (a) Sample noise feedback signal from LVDT - v2 from a stationary command and (b) distribution of the sample noise feedback signal with normal probability distribution fit to the data. 23
Figure 2.10 – (a) Sample noise feedback signal from LVDT – v3 from a stationary command and (b) distribution of the sample noise feedback signal with normal probability distribution fit to the data..... 23
Figure 2.11 – (a) Sample noise feedback signal from LVDT – v4 from a stationary command and (b) distribution of the sample noise feedback signal. 24

Figure 2.12 – General form of kernel regression estimation. 25
Figure 2.13 – Nadaraya-Watson kernel regression estimate and 95% confidence intervals for sample signals of Figure 2.8. 27
Figure 2.14 – Nadaraya-Watson kernel regression estimate and 95% confidence intervals for sample test. 27
Figure 2.15 – Example of bandwidth selection issues. 28
Figure 2.16 – Plot of sample test data with error bars against vertical noise signal distribution (no vertical movement)..... 30
Figure 2.17 – Test results for soil material Newhall#2, FC=10%, D_R=80%, vertical stress=1atm, saturation=0%, and OCR=1. (a) Plot of vertical strain at N=15 cycles vs. shear strain (b) in log-log scale. 31
Figure 3.1 – Gradation curves for Newhall#2. 32
Figure 3.2 – Test results of varying fines content for (a) D_R=60% and (a) D_R=80%. 36
Figure 3.3 – Plot of parameter *a* against (a) relative density and (b) fines content. 36
Figure 3.4 – Plot of parameter *b* against (a) relative density and (b) fines content. 37
Figure 3.5 – Global (e), intergranular (e_s), and interfine (e_f) void ratio versus fines content for Newhall#2 silty sand. 38
Figure 3.6 – Plot of parameter *R* against (a) relative density and (b) fines content. 40
Figure 3.7 – Plot of parameter *R* against cyclic shear strain amplitude for (a) relative density and (b) fines content. 41
Figure 3.8 – Test results of varying overburden at FC=10% for (a) D_R=60% and (a) D_R=80%. 41
Figure 3.9 – Plot of parameter $K_{\sigma\varepsilon}$ against vertical stress ratio for (a) relative density and (b) fines content. 42
Figure 3.10 – Plot of parameter *b* against vertical stress ratio for (a) relative density and (b) fines content. 42
Figure 3.11 – Plot of parameter *R* against vertical stress ratio for (a) relative density and (b) fines content. 43
Figure 3.12 – Plot of parameter *R* against cyclic shear strain amplitude for (a) FC=10 and (b) FC=50. 44
Figure 3.13 – (a) Test results of varying OCR at FC=10% (b) in log-log scale. Recall that data points below a vertical strain 2E-3% are not significantly different from zero per Section 2.3.4. 45
Figure 3.14 – Vertical strain profiles demonstrating dilation for (a) γ_c=0.15% and (b) γ_c=0.3%. 46
Figure 3.15 – Plot of parameter *R* against cyclic shear strain amplitude for FC=10. 47
Figure 3.16 – Plot of data comparing shear history effects for a sample with (a) D_R=45%, FC=0, and σ_v=2atm and (b) D_R=60% , FC=0, and σ_v=1atm. 48

1. INTRODUCTION

1.1 SEISMIC COMPRESSION

The focus of this research is on seismic compression. Seismic compression is defined as the accumulation of contractive volumetric strains in unsaturated soil from earthquake shaking. This type of ground deformation is a significant earthquake hazard and the estimation of settlement from seismic compression has become an integral component of modern geotechnical seismic design practice (SSC 1995; CGS 2005). However, there remains a lack of appropriate engineering methods for estimating such settlements.

This research is part of a long-term project directed towards developing Volumetric Strain Material Models (VSMM), which relate the shear strain demand applied to a soil element to the resulting volume change. VSMM models can be used with shear strains estimated from site response analysis to estimate the settlements from seismic compression.

1.2 LITERATURE REVIEW

The literature on seismic compression is categorized into case histories, previous research in seismic compression of clean sands, and previous research in seismic compression of sands with fines.

1.2.1 CASE HISTORIES

Several field case histories exist that document the settlements from seismic compression. These include the Jensen Filtration Plant shaken by the 1971 San Fernando earthquake (Pyke et al. 1975), two sites in Santa Clarita shaken by the 1994 Northridge earthquake (Stewart et al. 2004), damaged embankments from the 2001 Southern Peru

earthquake (Wartman et al. 2003), and the Kashiwazaki-Kariwa nuclear power plant shaken by the 2007 Niigata-ken Chuetsu-oki earthquake (Tokimatsu 2008).

The Joseph Jensen Filtration Plant site of Granada Hills, California was formed by a cut-and-fill operation. The compacted clayey sand fill was up to 17 m thick overlying 1.5-6 m of alluvium. The groundwater table was located in the alluvial layer, which liquefied from estimated peak horizontal accelerations of about 0.5-0.6 g. Recorded settlements were about 12.7 cm along a survey baseline as shown in Figure 1.1. However, Pyke et al. (1975) attributed much of the observed settlement to lateral spreading and estimated settlements due to seismic compression to be around 8.9-10.2 cm, which was about 0.7% of the fill thickness.

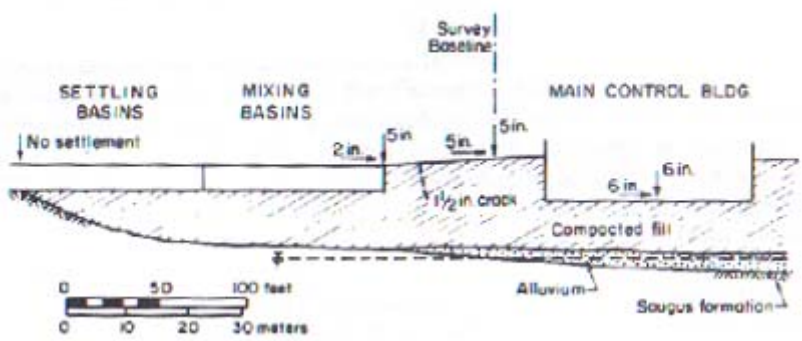

Figure 1.1 – Jensen Filtration Plant profile (Pyke et al. 1975).

In their analysis, Pyke et al. (1975) conducted a series of strain-controlled cyclic simple shear tests on the site fill material. Subsurface investigations revealed the clayey sand fill to be uniformly compacted with an average dry density of 1,937 kg/m3 and an average water content of 10%. This equated to a relative compaction of approximately 92%. The strain histories from their site response analysis were used to determine the equivalent number of uniform shear strain cycles, which they found to be five with a shear strain of two-thirds the peak value. Applying these values to the simple shear tests produced an estimate that was approximately one third of that observed in the field. Pyke et al. (1975) went on to conduct multi-directional shake table tests and found that

the total settlement caused by the combined horizontal motions are approximately equal to the sum of the settlements caused by the horizontal motions acting separately. Considering this, Pyke et al. (1975) applied a correction factor for multi-directional loading which increased their computed settlement to within the range of observed field settlements.

After the 1994 Northridge earthquake, two sites, Site A and Site B of Santa Clarita, California, were identified where the settlements from seismic compression could be reliably estimated. For Santa Clarita Site A, the soils consisted of a sandy clay and clayey sand fill up to 24 m thick underlaid by shallow alluvium and rock. Soil conditions show the fill generally being compacted to approximately 88% and dry of optimum. Stewart et al. (2004) estimated peak horizontal accelerations of 0.5-0.7 g with measured settlements of up to 22 cm from pre and post-earthquake surveys. For Santa Clarita Site B, the soils consisted of a silty sand fill 15-30.5 m thick lying over rock. Soil conditions indicate relative compactions of about 92-93% near the surface and about 95% at depth. Stewart et al. (2004) estimated peak horizontal accelerations of 0.8-1.2 g with measured settlements of 1.3-6.1 cm from pre and post-earthquake surveys. Figure 1.2 shows a plan of Site B indicating fill depths and measured settlements.

In their analysis, Stewart et al. (2004) used an approach that was similar to Pyke et al. (1975). For each site, they performed decoupled analyses of shear and volumetric strain. Shear strain was calculated using one-dimensional and two-dimensional ground response analyses, while volumetric strain was evaluated from shear strain using material-specific models derived from simple shear laboratory testing that incorporated important effects of fines content and as-compacted density and saturation. These strains were integrated over the height of the fill to estimate the total settlement from seismic compression. The computed settlements were in good agreement with the observed settlements at both Site A and Site B.

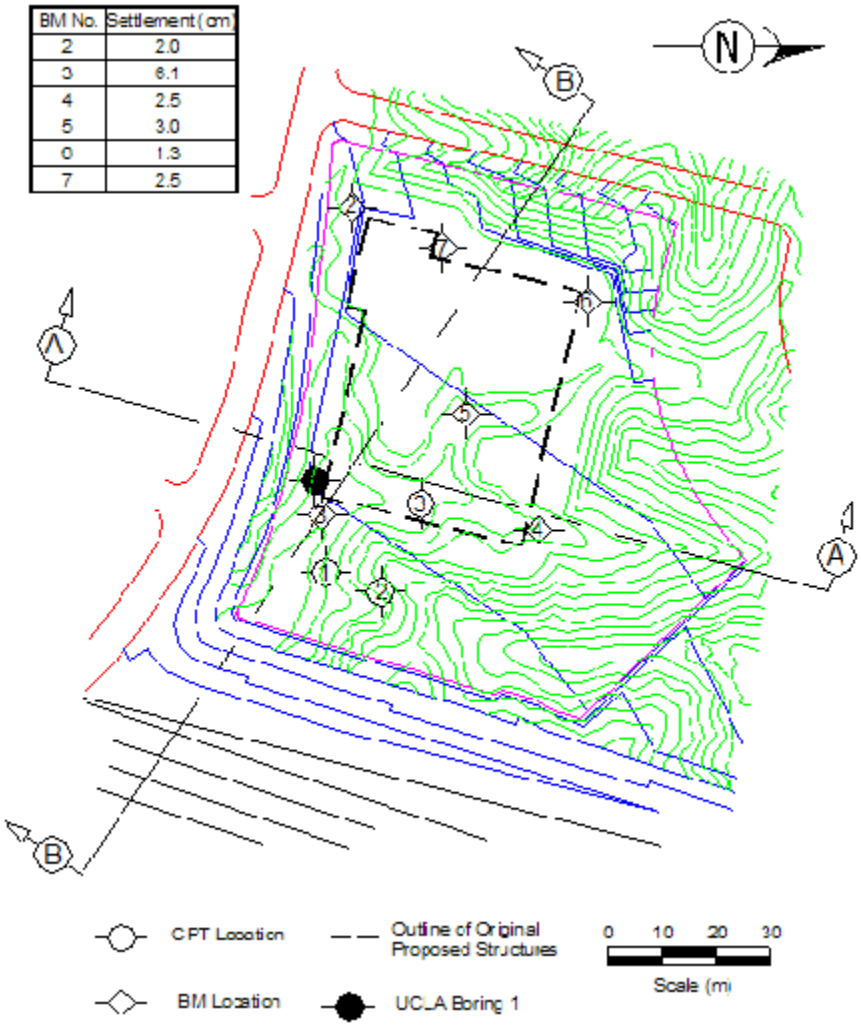

Figure 1.2 – Plan and settlement of Site B (Stewart et al. 2004).

In the 2001 Southern Peru earthquake, many highway embankment sites were damaged due to seismic compression and these damaged areas were almost entirely limited to fills. Wartman et al. (2003) describe these fills as consisting of gravelly, sandy, and silty soils with measured vertical deformations of 10 or more centimeters for 2-4 m high embankments. The investigators noted that vertical displacements were typically proportional to the height of the embankment and uniform across the road. Wartman et al. (2003) also observed seismic compression in a natural silty fine Aeolian sand overlaid by a highway road. Measured settlement was about 10-25 cm with lateral offsets of 5-10 cm. The investigators found newer embankments performed better than

older embankments and attributed it to modern construction compaction practices. Detailed back-analyses to evaluate the predictability of these deformations have not yet been completed.

In Japan, the Kashiwazaki-Kariwa nuclear power plant contained seven nuclear power generators directly founded on rock. Figure 1.3 shows an aerial photograph of the site. The soil used as compacted backfill surrounding the generators consisted mainly of sand 12-29.6 m thick. The groundwater table was lowered via a drainage system to reduce buoyancy effects on critical buildings and rose with distance from buildings. The groundwater and soil profile is shown in Figure 1.4. From ground motion recordings, Tokimatsu (2008) reported peak horizontal accelerations of 0.3-0.7 g, which caused estimated ground settlements on the average of 1-2% of fill thickness with the largest settlement in excess of 1.5 m. Ground deformations immediately surrounding the generators were much more significant indicating localized shear strains from soil-structure interaction.

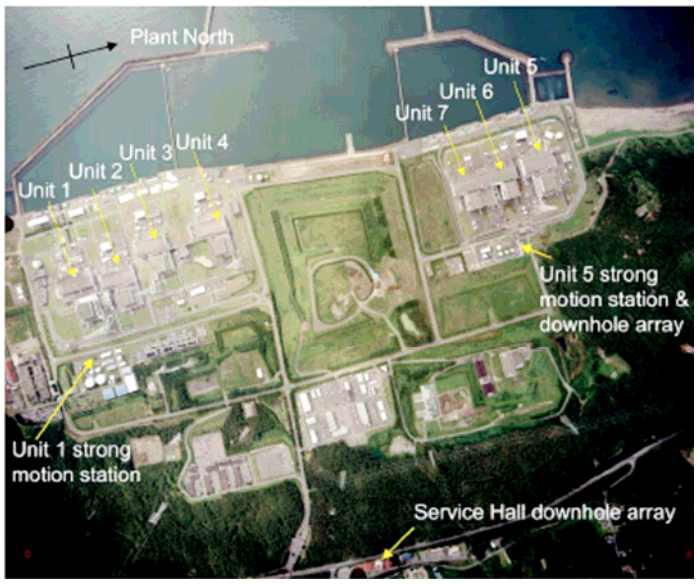

Figure 1.3 – Aerial photograph of Kashiwazaki-Kariwa nuclear power plant (Tokimatsu 2008).

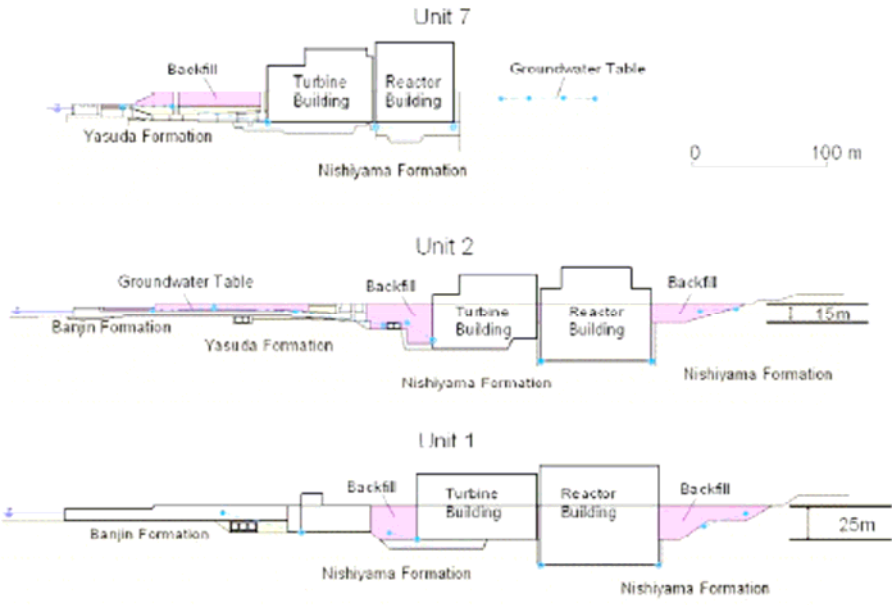

Figure 1.4 – Cross sections of Kashiwazaki-Kariwa nuclear power plant (Tokimatsu 2008).

1.2.2 PREVIOUS RESEARCH IN SEISMIC COMPRESSION OF CLEAN SANDS

The initial studies of seismic compression primarily concentrated on clean sands. Silver and Seed (1971) conducted strain-controlled simple shear testing with an NGI-type device on dry quartz sand (Crystal Silica No. 20). The researchers observed that volumetric strain was controlled by relative density, cyclic shear strain amplitude, and the number of uniform shear strain cycles. The researchers also found that volumetric strain was not significantly influenced by confining stress as shown in Figure 1.5. Shortly after, Youd (1972) confirmed these findings with Ottawa sand and shown that volumetric strain was independent from frequency of loading and saturation. Youd further observed a lack of compaction at shear strains less than 0.01%. This limiting value would come to be defined as the volumetric threshold shear strain (Vucetic 1994) with a range of 0.01-0.03% for sands (Hsu and Vucetic 2004).

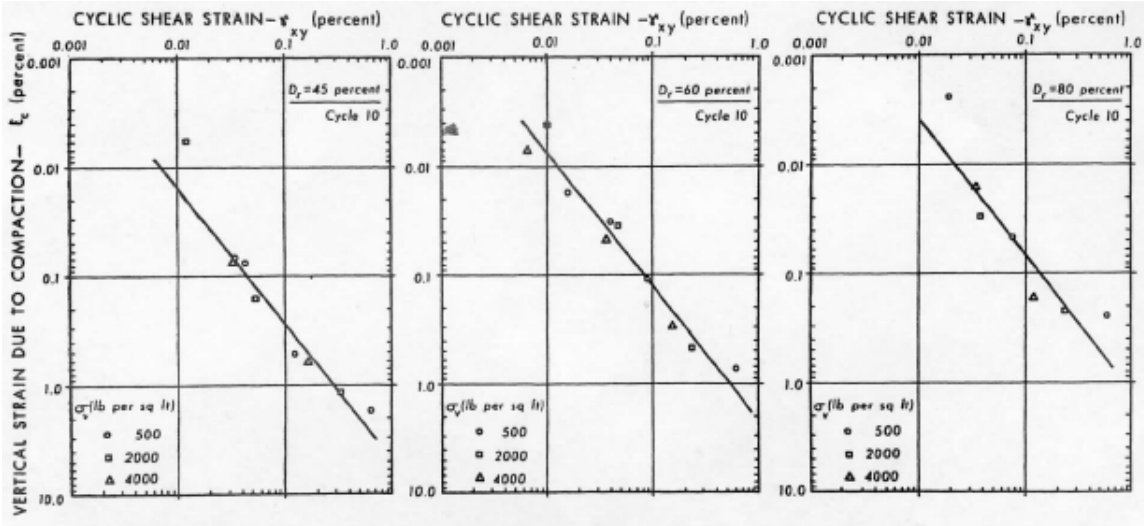

Figure 1.5 – Effect of surcharge on vertical strain (Silver and Seed 1971).

Seed and Silver (1972) took the results from Silver and Seed (1971) and suggested a procedure for estimating the settlement of dry sands during earthquakes that required a response analysis. To validate their procedure, the researchers conducted shake table tests on sandy layers placed at different relative densities and compared the results from their estimates. Although the researchers agreed that confining stress had little impact on seismic compression, their shake table test results, shown in Figure 1.6, appeared to indicate otherwise.

Subsequently, the Seed and Silver procedure would be modified by Pyke et al. (1975) to include multidirectional shaking effects. These multidirectional shaking effects were observed from shake table testing of Monterey No. 0 sand where the total settlement from dynamic loading was approximately equal to the sum of the settlements caused by the components acting separately as shown in Figure 1.7.

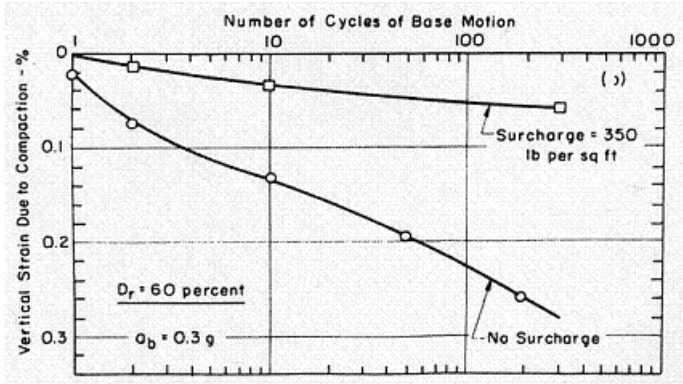

Figure 1.6 – Effect of surcharge on vertical strain (Silver and Seed 1971).

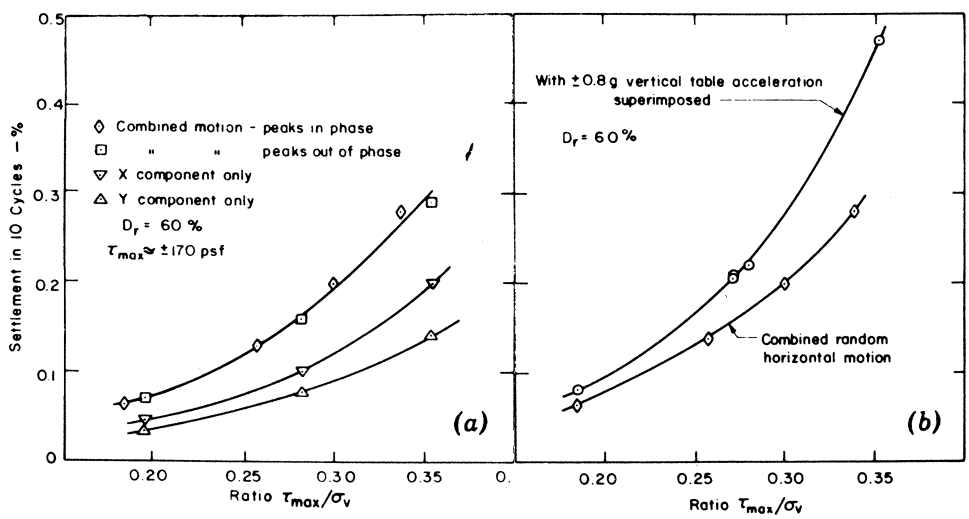

Figure 1.7 – Comparison of settlements under (a) components and combined random motions and (b) in three-dimensional shake table tests (Pyke et al. 1975).

Based on the laboratory test data on dry clean sand by Silver and Seed (1971), Tokimatsu and Seed (1987) developed a simplified procedure for estimating settlements from seismic compression. This procedure linked volumetric strain, shear strain, and a standard penetration test $(N_1)_{60}$ blow count for a magnitude 7.5 earthquake and is shown in Figure 1.8a. The Tokimatsu and Seed VSMM uses the relation in Seed et al. (1983) to link a magnitude 7.5 earthquake to earthquakes of other magnitudes through an equivalent number of cycles. This equivalent number of cycles is then used to determine the estimated settlement through Figure 1.8b. Tokimatsu and Seed also

recommended doubling the estimated settlements to account for multidirectional shaking effects (Pyke et al. 1975).

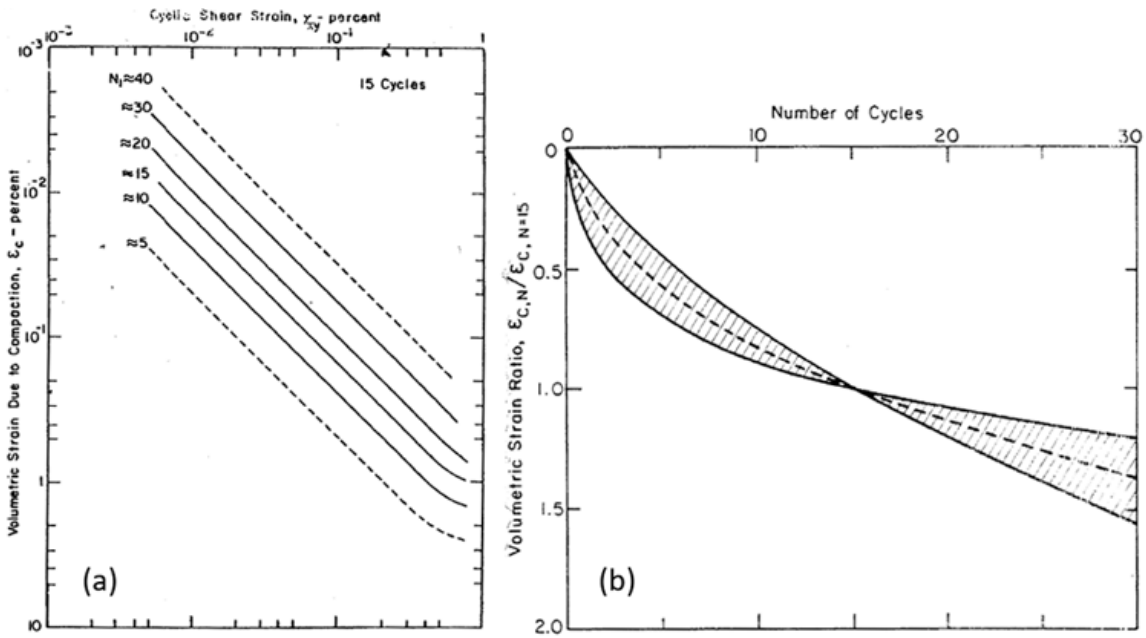

Figure 1.8 – Simplified procedure for dry sands: (a) relationship between volumetric strain, shear strain, and penetration resistance and (b) relationship between volumetric strain ratio and number of cycles (Tokimatsu and Seed 1987).

Recently, Duku et al. (2008) investigated the effects of a variety of compositional and environmental factors on volumetric strain at 15 uniform shear strain cycles. Based on laboratory simple shear testing of 16 sands, the researchers observed that relative density and overburden were directly correlated to seismic compression and reinforced previous findings that loading frequency and saturation had little effect on vertical strains. Principal findings for clean sands include (i) vertical strains are less than previous researchers, (ii) vertical strains increase as relative density decreases, (iii) vertical strains decreased as overburden increased, which is contrary to previous investigators, (iv) OCR has an effect on vertical strains, but is not present at lower overburden pressures and was not analyzed further as most soils that are overconsolidated are near the surface where overburden pressures are relatively low, and (v) a lack of saturation effects and

frequency of loading effects. These results are also presented in a 2007 NEHRP final project report by the PI.

1.2.3 PREVIOUS RESEARCH IN SEISMIC COMPRESSION OF SANDS WITH FINES

Previous research on seismic compression behavior of soils with fines has been presented by Pyke et al. (1975), Whang et al. (2004), and Whang et al. (2005). Pyke et al. (1975) performed a limited number of cyclic simple shear tests on well-graded clayey sand. This material was taken from the Jensen Filtration Plant case history study described in section 1.2.1. The researchers tested soil samples at two dry densities of 1.78 and 1.94 g/cm^3, with an average water content of 10%. Whang et al. (2004) performed cyclic simple shear testing on four soils taken from the two sites described in section 1.2.1 by Stewart et al. (2004). These materials contained high fines contents, FC = 40–54% with plasticity indices, PI = 2–15, and were prepared to relative compactions of 84 to 96%. Their findings showed lower levels of vertical strain relative to clean sands at similar loadings and relative compactions and is illustrated in Figure 1.9.

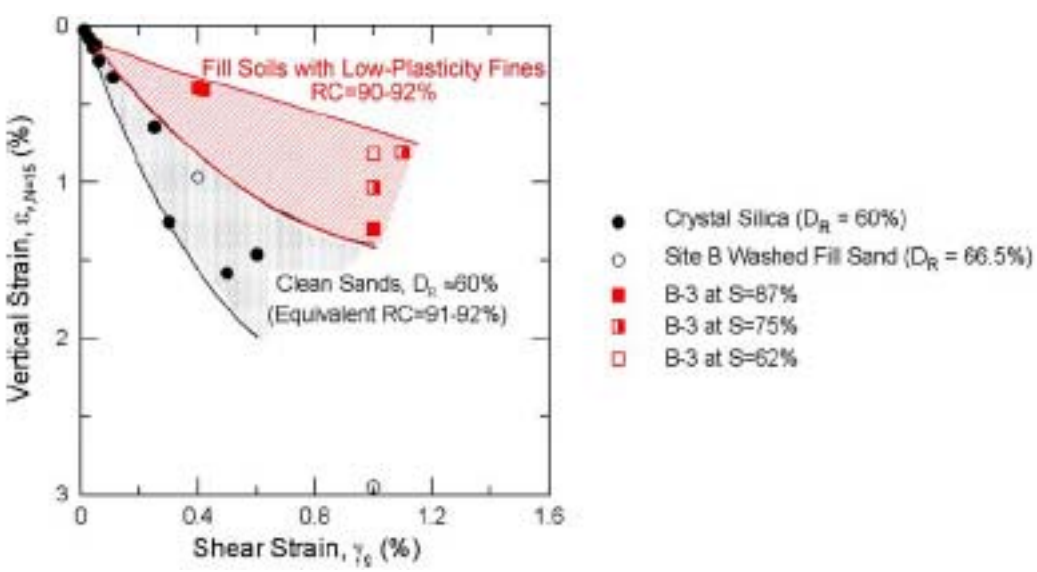

Figure 1.9 – Comparison of cyclic vertical strain behavior for fill soils with low-plasticity fines and clean sands (Whang et al 2004).

Their tests also showed that compacted plastic soils have lower seismic compression when compacted at high saturation (wet of line of optimums) than when compacted at lower saturations. Soils with low plasticity fines (PI~2) did not show a significant effect of saturation.

Later on, Whang et al. (2005) investigated the effects of density, saturation, and fines content on the seismic compression behavior of several synthetic non-plastic silty sands, where the fines were rock-flour. They found intermediate levels of saturation, S~30%, produced vertical strains that were less than samples with S=0% and S>60%. Matric suction testing revealed that matric suction was high for S~30% and thus appeared to be correlated to the reduction in vertical strains. The investigators also found increasing fines content increased vertical strains under constant relative compaction. These effects are summarized in Figure 1.10.

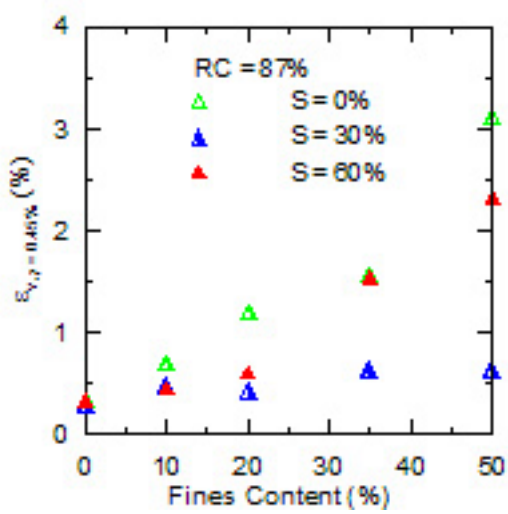

Figure 1.10 – Fines content and saturation effects on seismic compression behavior (Whang et al. 2005).

Note that whereas the earlier studies by Pyke et al. (1975) and Whang et al. (2004) found that moderate to low plasticity fines decreased seismic compression relative to clean sand, Whang et al. (2005) found that nonplastic fines increased seismic compression relative to comparable clean sands.

1.3 PRESENT STUDY

Largely because of the significant damage that occurred to structures as a result of seismic compression induced by the 1994 Northridge earthquake and subsequent foreign events, there has been increasing demand within the engineering profession for seismic compression analysis procedures that can be utilized in practice. The state-of-practice method for seismic compression analysis consists of a procedure by Tokimatsu and Seed (1987), updated by the Duku et al. (2008) volumetric strain material model (VSMM), which is intended for application to clean sands as described in Section 1.2.2. Accordingly, there is a major research need for laboratory testing to establish volumetric strain material models that cover a broad range of soil types and characteristics. The principal objectives of this research are to:

- To better understand the seismic compression susceptibility of sands with low-plasticity fines, with a special focus on the effects of overburden stress and stress history in addition to the traditional factors of relative density and demand parameters (shear strain amplitude and number of cycles).
- To document the uncertainty in the data points that are used to develop VSMM, which is particularly critical for the small strain range.

These objectives are accomplished through:

- Statistical analysis of test data and development of protocols for defining confidence intervals on data points (Chapter 2).
- Laboratory testing of mixtures of sand materials and low plasticity fines to test volumetric strains as functions of N, γ_c, OCR, FC, PI, total overburden pressure, and matric suction (Chapter 3).

2. DATA ANALYSIS

2.1 UCLA DIGITALLY CONTROLLED SIMPLE SHEAR DEVICE

The UCLA digitally controlled simple shear device (DC-SS) used in the current and past research on seismic compression at UCLA is described in Duku et al. (2007). This device, shown in Figure 2.1, was used by Whang et al. (2004, 2005) and by Duku et al. (2006, 2008). A limitation of the device is the inability to reliably measure small amplitude cyclic shear strains due to system noise as shown in Figure 2.2. An examination of this system noise and how it affects system output is presented in the following sections.

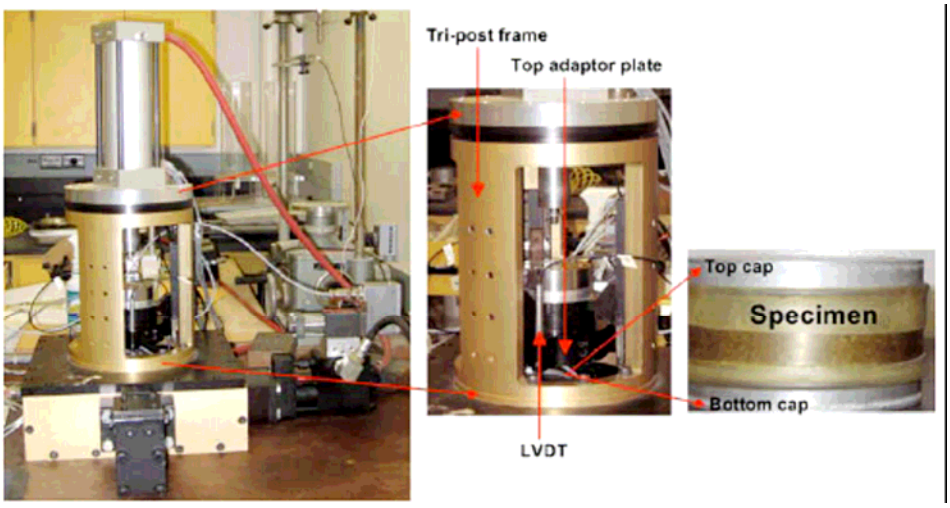

(a) (b) (c)

Figure 2.1 – Photographs of UCLA DC-SS showing (a) overview, (b) view of frame and adapter plate, and (c) soil sample in wire-reinforced membrane between caps (Duku et al. 2007).

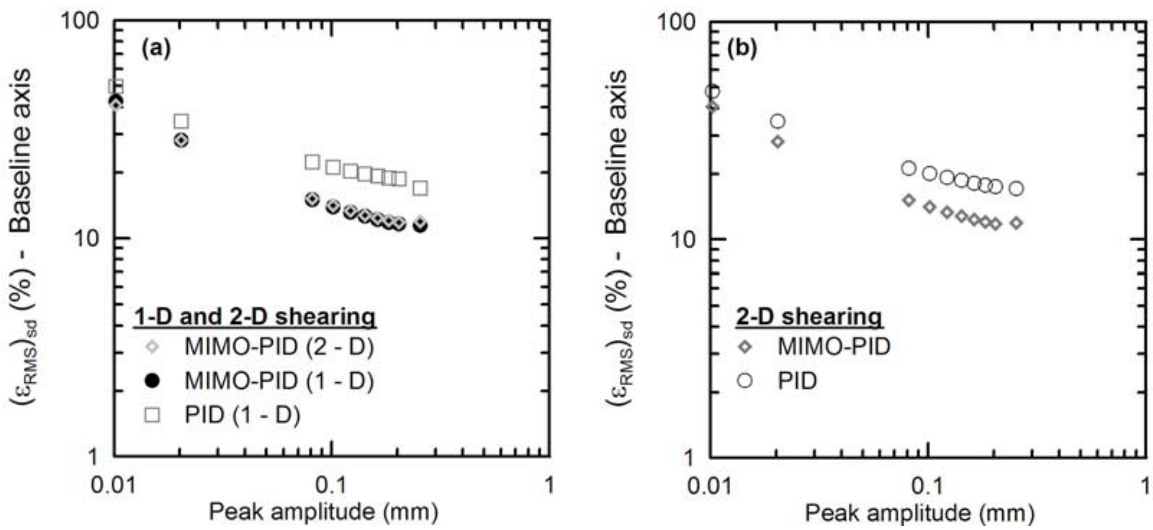

Figure 2.2 – Normalized root mean square of tracking errors for (a) unidirectional and (b) multidirectional broadband command signals of different amplitude (Duku et al. 2007).

2.2 CYCLIC SHEAR STRAIN VARIABILITY

The DC-SS, similar to other simple shear devices, can impart a horizontal sinusoidal motion to the base of the soil specimen. The DC-SS does this by comparing the feedback signal from a horizontal linear variable displacement transducer (LVDT), which measures the actual physical displacement of the specimen, with the command signal, which indicates where the specimen should be at a particular point in time. A sample signal profile is shown Figure 2.3. Tracking errors result when these two signals do not match and are calculated using the normalized root mean square error:

$$\varepsilon_{NRMS,tracking} = \sqrt{\frac{\sum_{i=1}^{n}\left(y_{i,signal} - y_{i,command}\right)^2}{\sum_{i=1}^{n}\left(y_{i,signal}\right)^2}} \tag{2.1}$$

where n = number of data points; $y_{i,signal}$ = feedback signal data; $y_{i,command}$ = command signal data; $y_{\max,signal}$ = maximum feedback signal value; and $y_{\min,signal}$ = minimum

feedback signal value. This is the same error function used by Duku et al. (2007) except that the denominator has been changed from the command signal to the feedback signal, because cases of 0-command signals are considered.

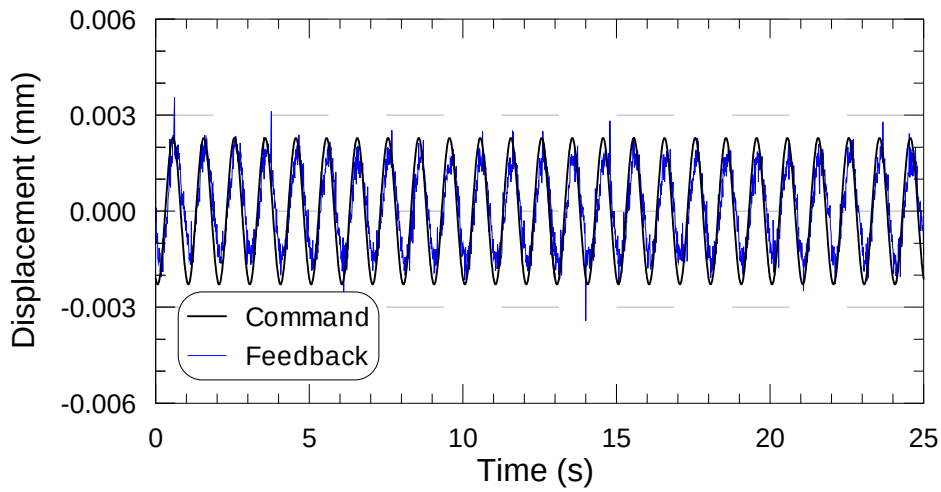

Figure 2.3 – Sample sinusoidal wave command and corresponding feedback.

2.2.1 NOISE FROM HORIZONTAL MEASUREMENTS WITH ZERO COMMAND SIGNAL

Figure 2.4 shows the first 25 seconds of two sample outputs from the axis 1 horizontal linear variable displacement transducer (LVDT – h1) when the DC-SS is given a stationary command (amplitude = 0). Since the system is essentially stationary, the feedback signal is considered noise. Figure 2.5 shows the distribution of the complete noise feedback signals along with a normal distribution fit to each dataset. Both sets of figures suggest the noise feedback signal is normally distributed with zero mean and standard deviation = 0.0003-0.0004 mm.

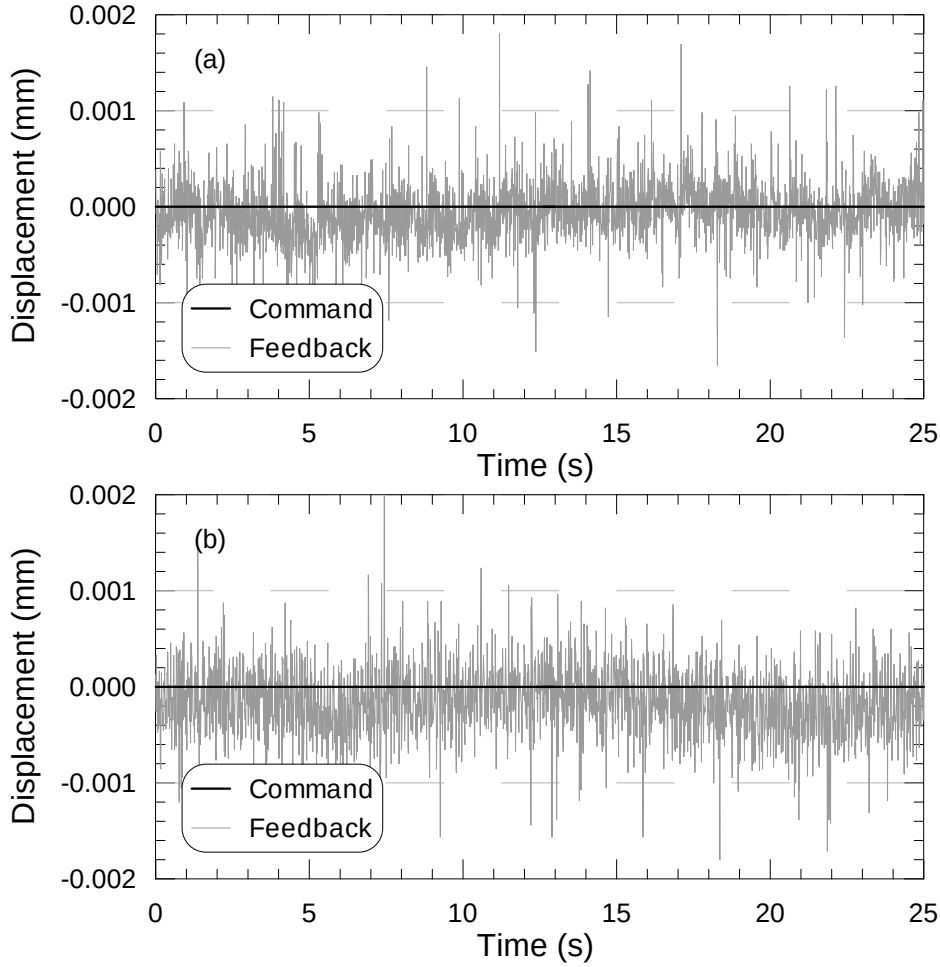

Figure 2.4 – Sample noise feedback signal from horizontal LVDT for (a) trial 1 and (b) trial 2.

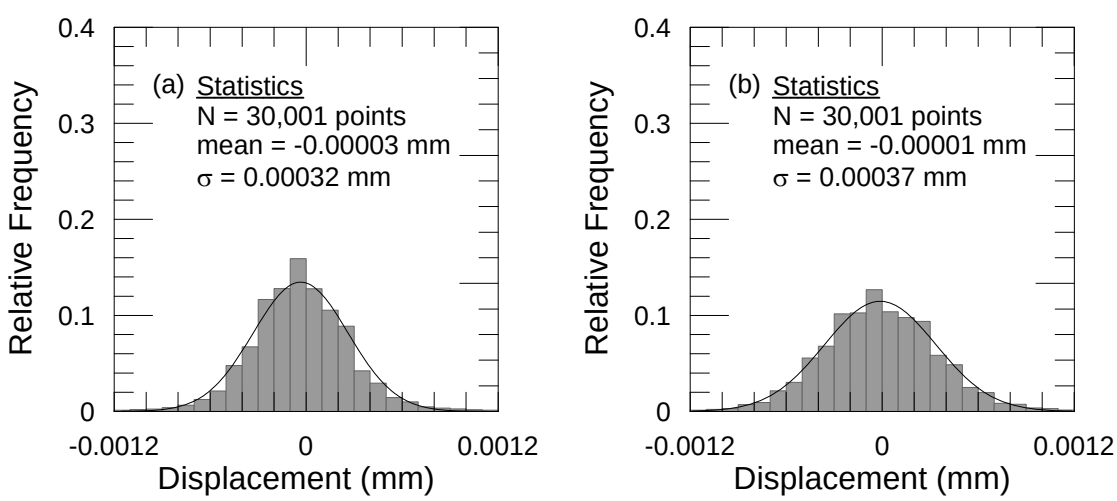

Figure 2.5 – Distribution of sample noise feedback signal and normal probability distribution fit to the data for (a) trial 1 and (b) trial 2.

2.2.2 QUANTIFICATION OF HORIZONTAL MEASUREMENT VARIATION

As shown in Figure 2.3, noise introduces scatter to cyclic displacement amplitudes. This becomes especially true when the signal amplitude approaches the noise amplitude. Several statistical techniques were considered to distinguish noise from the displacement actually experienced by the specimen.

2.2.2.1 SPECTRAL ANALYSIS

One set of statistical techniques appropriate for extracting amplitudes from noisy sinusoidal waveforms involves spectral analysis. These techniques involve the statistical properties of the Fourier series, which is an alternate representation of time domain data in the frequency domain through a Fourier transform or basis function. The transform deconstructs a periodic function into a sum of sinusoidal functions. In this case, the time-displacement data is transformed into frequency-Fourier pair data:

$$a_k = \frac{2}{n}\sum_{i=1}^{n} f(t_i)\cos(\omega_k t_i) \tag{2.2}$$

$$b_k = \frac{2}{n}\sum_{i=1}^{n} f(t_i)\sin(\omega_k t_i) \tag{2.3}$$

where n = number of data points; $f(t_i)$ = data at points; ω_k = frequency of interest; and (a_k, b_k) = Fourier pairs. The Fourier pairs can be used to reconstruct the waveform via:

$$R_k = \sqrt{a_k^2 + b_k^2} \tag{2.4}$$

$$\theta_k = \tan^{-1}\left(\frac{-b_k}{a_k}\right) \tag{2.5}$$

$$\hat{f}(t) = \sum_{i=1}^{n} R_k \cos(w_k t_i + \theta_k) \tag{2.6}$$

where R_k = amplitude for frequency k; θ_k = phase for frequency k; $\hat{f}(t)$ = horizontal displacement estimate. Modern spectral analysis uses the Fast-Fourier transform, which is similar to the transformations previously presented, but Fast-Fourier transform is partially limited by the fact that the data must be modified in order to yield results at the frequencies of interest. Assuming the noise is additive to the signal and normally distributed with mean 0 and variance σ^2, the probability distribution for the Fourier coefficients can be calculated by (Thibos 2004):

$$\frac{(\hat{a}_k - a_k)^2 + (\hat{b}_k - b_k)^2}{\left(2\sigma^2/n\right)} \sim \chi_2^2 \tag{2.7}$$

where (a_k, b_k) = true Fourier pair; σ^2 = variance of the noise; and χ_2^2 = Chi-square distribution with 2 degrees of freedom. This variable is chi-square distributed because the sum of two squared normally distributed random variables is chi-square distributed. The plot of R_k against frequency, ω_k, is termed an amplitude spectrum. For example, Figure 2.6 is the amplitude spectrum of Figure 2.3. The command signal is also shown for comparison. The spectral estimates do not match away from the control frequency of 1 Hz due to noise.

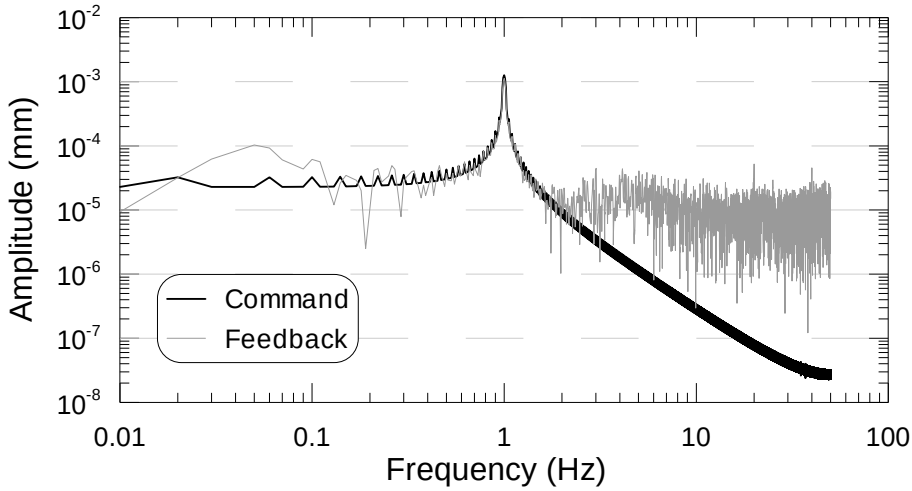

Figure 2.6 – Frequency domain representation of sample feedback and command signal.

2.2.2.2 REGRESSION

Another technique involves transforming the data prior to performing linear regression. Assuming the signal data can be modeled in the form:

$$Y = A\cos(\omega t + \phi) \tag{2.8}$$

where:

Y = horizontal displacement (signal data)

A = amplitude estimate

ω = frequency of interest

t = time (signal data)

ϕ = phase

Note that A is analogous to R_k in the previous section; the difference is that R_k is the Fourier amplitude of the data whereas A is the estimated amplitude from regression analysis. By letting $X = \cos(\omega t + \phi)$, the model then becomes $Y = AX$. Performing a least squares regression for the slope parameter, A, yields an estimated amplitude for

the signal. Using this value of A, an estimate of the feedback signal is obtained, which is denoted Y in Eq. (2.8). A residual can be calculated between the data ($y_{i,signal}$) and the model estimate,

$$R(t) = y_{i,signal}(t) - Y(t) \tag{2.9}$$

Assuming residuals at different points in time $R(t)$ are statistically independent but have the same underlying normal distribution (mean and standard deviation), confidence intervals for the estimated slope parameter will then be:

$$A = \hat{A} \pm t_{crit} S_{slope} \tag{2.10}$$

where:

t_{crit} = critical t-value for N-1 degrees of freedom

N = number of data points

S_{slope} = standard deviation of the slope

$$= \sqrt{\frac{\Sigma(y-\hat{y})^2}{(N-1)}} \Bigg/ \sqrt{\Sigma(x-\hat{x})^2}$$

Even if the residuals are not completely independent due to the control algorithm, Eq. (2.10) should give a reasonable confidence bound nonetheless since any noise correlations between peaks will not be overly severe.

2.2.3 RESULTS OF HORIZONTAL MEASUREMENT ANALYSIS

To compare the accuracy and appropriateness of the aforementioned methods, the normalized root mean square error and the 95% confidence interval range are used as error metrics. The normalized root mean square error was defined in Eq. (2.1), with the estimated signal used in place of the command signal. Results from sample tests are

shown in Figure 2.7. Figure 2.7a shows the normalized root mean square error for each amplitude estimate from both spectral analysis and linear regression. The plot shows both methods estimate the same amplitude with better fits as the amplitude increases. Figure 2.7b compares the 95% confidence interval range, which is simply the difference between the upper and lower bounds, against the amplitude estimate. The plot shows that for the linear regression method, the 95% confidence interval range increases as the amplitude estimate increases, while the spectral analysis method yields a constant range for all amplitudes.

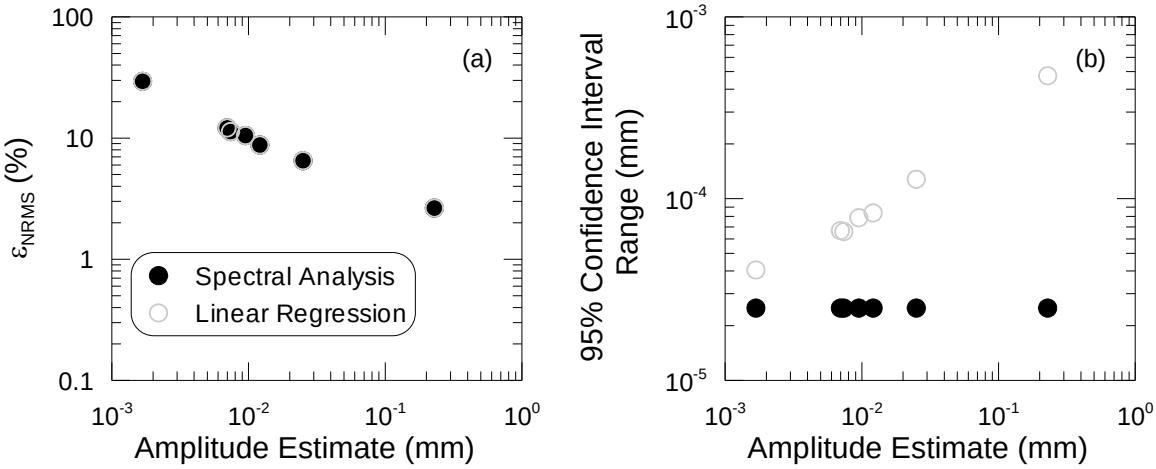

Figure 2.7 – Error metrics from sample tests for (a) normalized root mean square error and (b) 95% confidence interval range.

Even though the methods yielded essentially the same amplitude estimates, the results show that spectral analysis produces relatively narrower confidence intervals, which implies a decrease in variability. However, since both methods produce the same amplitude estimates, the residuals from one method are not necessarily more variable than the other method. For purposes of DC-SS horizontal displacement analysis, spectral analysis will be used from now on even though it is computationally intensive relative to the linear regression method.

2.3 VERTICAL STRAIN VARIABILITY

There are three LVDTs to measure vertical displacement around the sample. Figure 2.8 shows the vertical displacement from a test conducted with small horizontal displacement amplitude. The plot indicates that one of the vertical LVDTs has a lower resolution than the other two and has relatively noisy displacement histories, making it difficult to evaluate end-of-cycle displacement. Additionally, the noise makes it difficult to evaluate if a change in height did or did not occur. These two issues will be addressed in evaluating vertical strain variability.

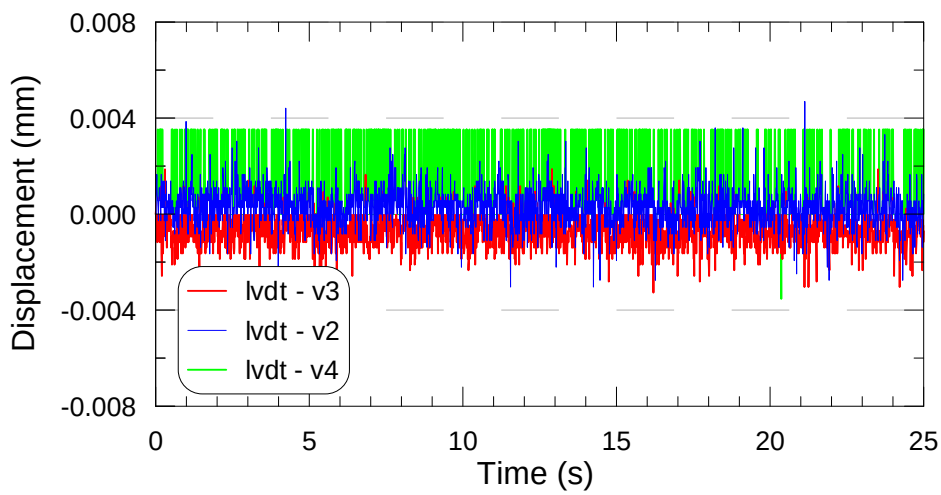

Figure 2.8 – Sample vertical displacement output.

2.3.1 NOISE FROM VERTICAL MEASUREMENTS

To evaluate noise levels from the vertical LVDTs (denoted v2, v3, and v4), a stainless steel cylinder about 60 mm in height was placed into the DCSS to displace the vertical LVDTs. A stationary command was issued and feedback signals from the vertical LVDTs were recorded. Sample feedback signals from LVDT – v2, v3, and v4 are shown in Figures 2.9a, 2.10a, and 2.11a respectively with their distributions shown in Figures 2.9b, 2.10b, and 2.11b. Figure 2.9 and Figure 2.10 show that the noise for LVDT – v2 and v3 appear to be normally distributed with a mean of zero. Figure 2.11 shows the noise for LVDT –

v4 essentially takes on one of two values when the DC-SS is stationary. The difference in resolution between LVDT – v4 and LVDTs – v2 and v3 is due to the type of analog-to-digital converter channel used. LVDT – v4 uses a 12-bit channel whereas LVDTs – v2 and v3 use 16-bit channels, thereby producing higher resolution signals for the fixed range of displacement.

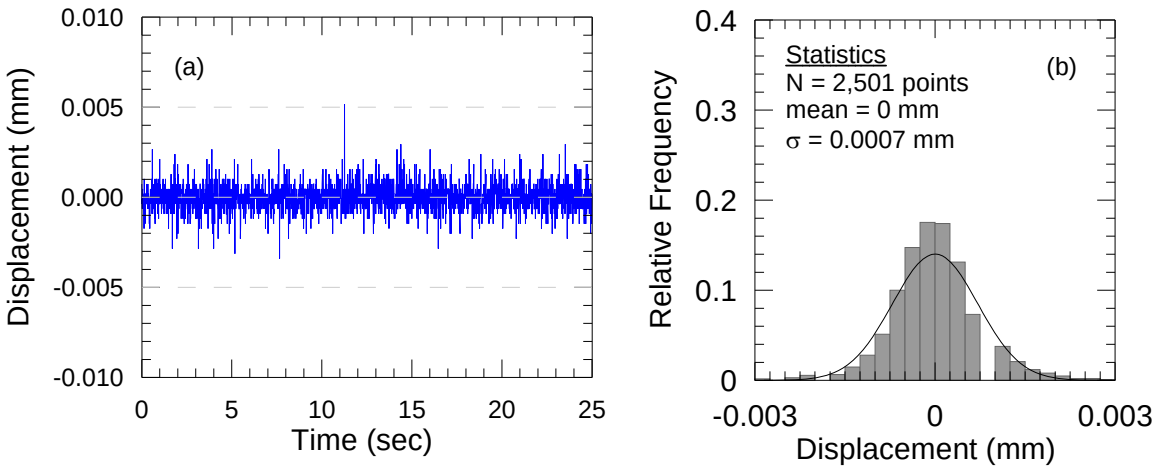

Figure 2.9 – (a) Sample noise feedback signal from LVDT - v2 from a stationary command and (b) distribution of the sample noise feedback signal with normal probability distribution fit to the data.

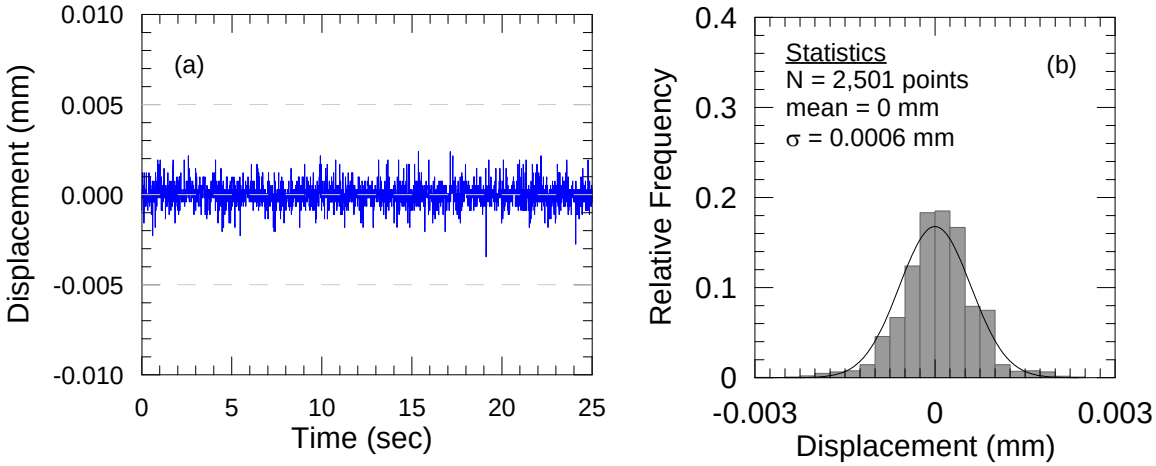

Figure 2.10 – (a) Sample noise feedback signal from LVDT – v3 from a stationary command and (b) distribution of the sample noise feedback signal with normal probability distribution fit to the data.

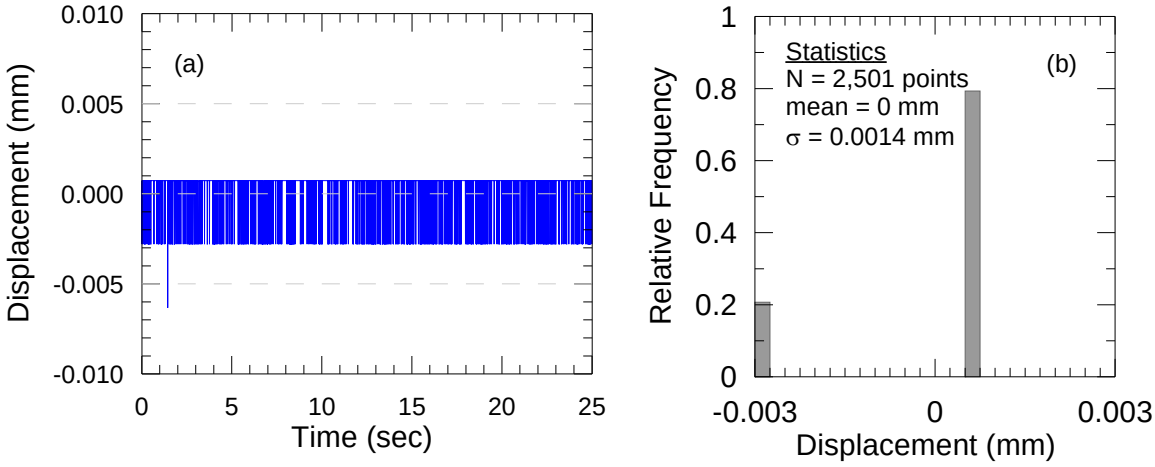

Figure 2.11 – (a) Sample noise feedback signal from LVDT – v4 from a stationary command and (b) distribution of the sample noise feedback signal.

2.3.2 QUANTIFICATION OF VERTICAL MEASUREMENT VARIATION

Since vertical displacements are measured through three different channels, an obvious method to estimate specimen vertical displacement is to take the statistical mean of the three measurements. However, because each of the LVDTs has the potential for error (defined in previous section), their average will also have non-zero error at any point in time. Those errors may be significant when the displacements are small (near the noise level). To minimize the effects of such erroneous displacements, nonparametric regression is considered. Nonparametric regression provides an effective means by which complex displacement patterns occurring over a wide range of values can be captured without the constraint of an assumed functional form.

One type of nonparametric regression is kernel regression, or kernel smoothing. Kernel smoothing generally utilizes locally weighted averages of the data defined by a kernel. The kernel is dependent on the selected bandwidth and kernel function. The bandwidth and kernel function determine how much to weigh different values in constructing an estimate at a particular point in time. Figure 2.12 illustrates how kernel regression estimation generally works and the variables considered.

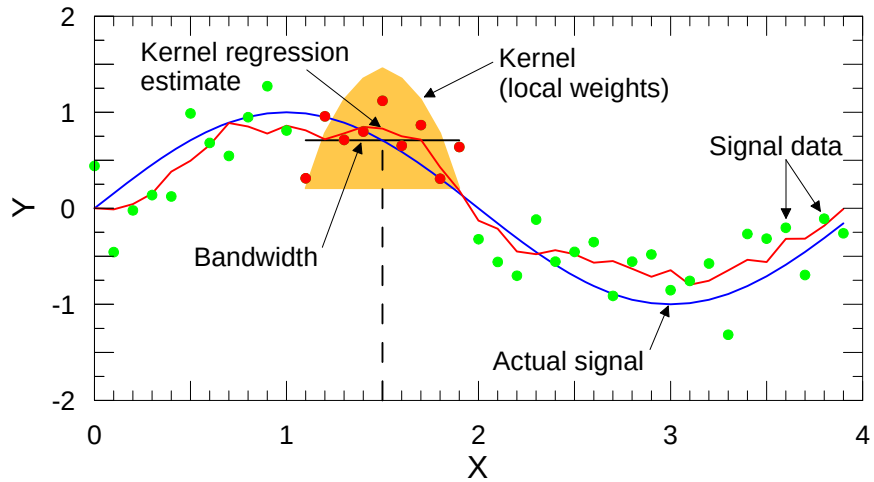

Figure 2.12 – General form of kernel regression estimation.

For this study, the Nadaraya-Watson kernel regression function estimator (Nadaraya 1964, Watson 1964) is used:

$$\widehat{m}_h(x) = \frac{\sum_{i=1}^{n} K_h(x - X_i) Y_i}{\sum_{i=1}^{n} K_h(x - X_i)} \tag{2.11}$$

where:

h = bandwidth, length of time window

n = number of data points within bandwidth

$$K_h(\mu) = \frac{K\left(\frac{\mu}{h}\right)}{h}$$

$K(u)$ = kernel function

$$= \frac{1}{\sqrt{2\pi}} e^{-\frac{1}{2}u^2} \quad \text{(Gaussian)}$$

with point-wise confidence intervals defined by:

$$\widehat{m}_h(x) \pm z_{1-\alpha/2}\sqrt{\frac{\|K\|_2^2\,\widehat{\sigma}^2(x_i)}{nh\hat{f}_h}} \tag{2.12}$$

where:

$$z_{1-\alpha/2} = (1-\alpha/2)\text{-quantile of the standard normal distribution}$$

$$\|K\|_2^2 = \int_{-\infty}^{\infty}[K_h(x)]^2 dx$$

$$\widehat{\sigma}^2(x) = \frac{1}{n}\sum_{i=1}^{n} W_{hi}(x)(Y_i - \widehat{m}_h(x))^2$$

$$W_{hi}(x) = \frac{K_h(x - X_i)}{\hat{f}_h(x)}$$

$$\hat{f}_h(x) = \frac{1}{nh}\sum_{i=1}^{n} K\left(\frac{x - X_i}{h}\right)$$

Although kernel smoothing is an effective method, simple kernel estimates are substantially biased near the boundaries. As the dependent variable approaches a boundary of the data (beginning or end of test), the kernel weights are no longer symmetric. This results in biased estimates at the boundary. For this investigation, there is initial seating load data before the simple shear load is applied, therefore extending the initial boundary before simple shear testing begins. Due to high resolution and multiple LVDTs, the end boundary can be calculated asymmetrically without a significant loss of accuracy. Selecting a narrow bandwidth also lessens the boundary effects. The tradeoff in selecting a smaller bandwidth is larger variance, which widens confidence intervals.

For the DC-SS, all three vertical LVDT signals are considered simultaneously. By doing this, the Nadaraya-Watson estimator would basically average the three signals and calculate a weighted average over time of these averages. The results of applying the Nadaraya-Watson kernel regression estimator to the sample signals in Figure 2.8 are shown in Figure 2.13. This estimate used a bandwidth, h=0.50 seconds and gave

relatively narrow confidence intervals. The results of applying the Nadaraya-Watson kernel regression estimator to a large amplitude test are shown in Figure 2.14.

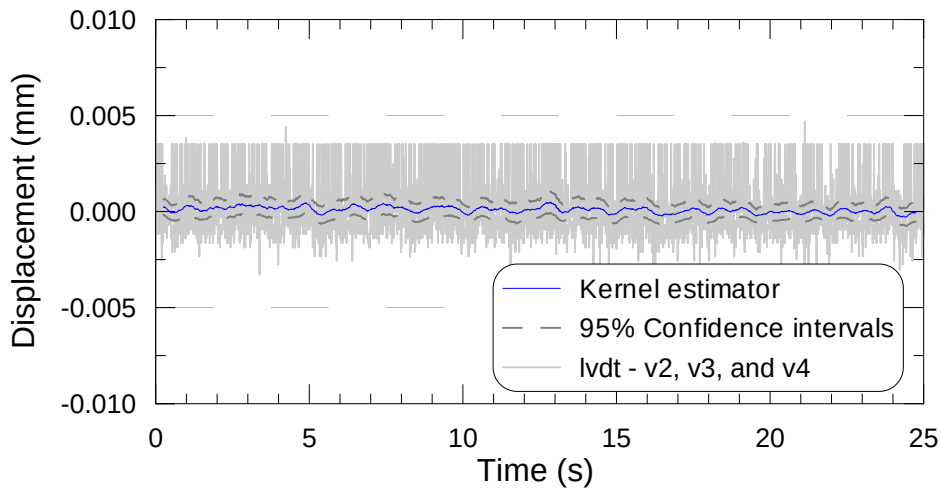

Figure 2.13 – Nadaraya-Watson kernel regression estimate and 95% confidence intervals for sample signals of Figure 2.8.

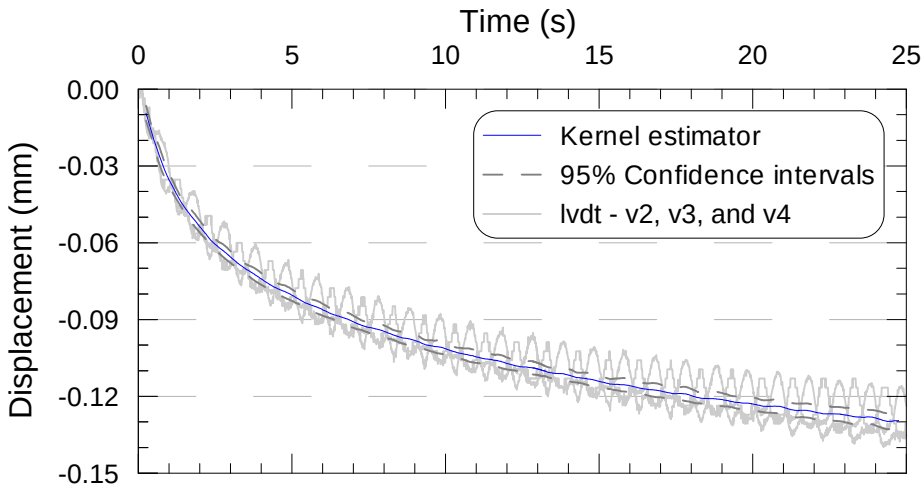

Figure 2.14 – Nadaraya-Watson kernel regression estimate and 95% confidence intervals for sample test.

2.3.3 RESULTS OF VERTICAL MEASUREMENT ANALYSIS

The most important variable in nonparametric regression is bandwidth selection (Härdle 1990). Figure 2.15 is an exaggerated example that illustrates the main issue in

bandwidth selection. Choosing a large bandwidth incorporates more data into the regression thereby reducing variance, but the side effect is an increase in bias, which is defined here as the difference between the ideal estimate and the computed estimate. The blue symbol shown in Figure 2.15 represents the estimate from a large bandwidth defined by the blue dashed lines. Choosing a small bandwidth incorporates less data into the regression thereby reducing the potential bias, but has the effect of increasing variance, which is shown with the red symbol and red dashed lines. It can be readily seen that the bias from the larger bandwidth is much greater than that from the smaller bandwidth.

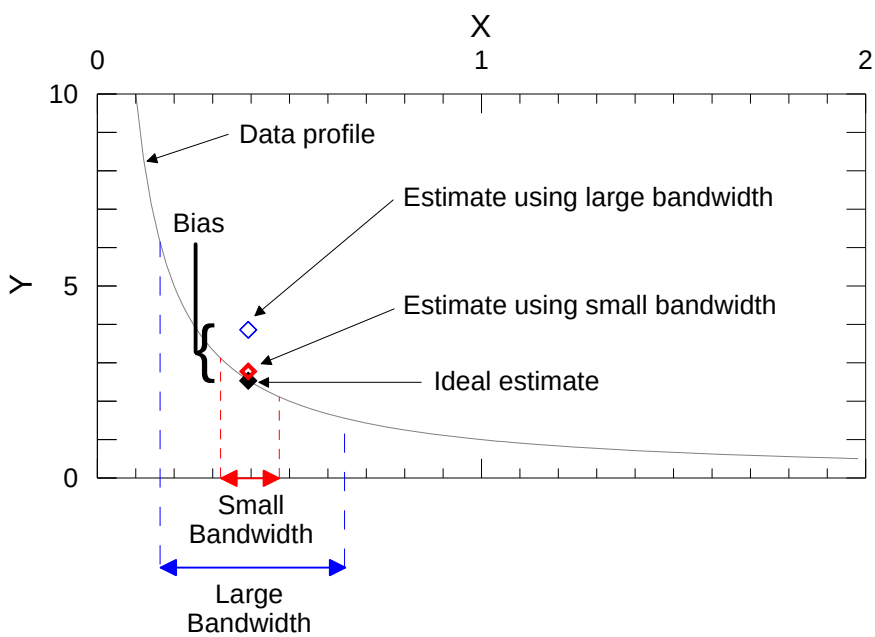

Figure 2.15 – Example of bandwidth selection issues.

For a consistent framework in the analysis of DC-SS test results, a bandwidth was selected that balances bias and variability. This was done by comparing the average point-wise 95% confidence interval range against the average root mean square error. The average root mean square error is calculated by:

$$\varepsilon_{RMS,v} = \frac{1}{n}\sum_{i=1}^{n}\sqrt{\frac{1}{3}\left[\left(y_{i,LVDT-v2} - \hat{m}_{h,i}\right)^2 + \left(y_{i,LVDT-v3} - \hat{m}_{h,i}\right)^2 + \left(y_{i,LVDT-v4} - \hat{m}_{h,i}\right)^2\right]} \quad (2.13)$$

where n = number of data points; $y_{i,LVDT-v2}$ = signal data from LVDT-v2; $y_{i,LVDT-v3}$ = signal data from LVDT-v3; $y_{i,LVDT-v4}$ = signal data from LVDT-v4; and $\hat{m}_{h,i}$ = nonparametric regression estimate at time *i*. Minimizing the difference between the average 95% confidence interval range and the average root mean square error would result in a bandwidth that balances variability with loss of accuracy by ensuring that at least half of the bias is taken into account in the confidence interval. For DC-SS testing at a frequency of 1-Hz, this bandwidth was calculated to be approximately between 0.4 to 0.6 seconds. For subsequent analysis, we select a bandwidth of 0.5 seconds.

2.3.4 UTILIZATION OF VERTICAL DISPLACEMENT ERROR MEASUREMENT TO EVALUATE DISPLACEMENTS AT THE VOLUMETRIC THRESHOLD SHEAR STRAIN

It is difficult to distinguish whether a DC-SS sample has undergone volume change when the vertical displacements approach the noise amplitude. However, armed with the data and methods described previously, a framework to define the volumetric threshold shear strain can be developed. Volumetric threshold shear strain, γ_{tv}, is defined as the amplitude of shear strain in cyclic loading tests below which no volume change occurs. An example is shown in Figure 2.16. This figure shows actual test data in blue with corresponding error bars computed from the methods described in previous sections. The "H"s at each data point represent the 95% confidence intervals for vertical displacement, where the vertical lines at the ends delimit the interval. These lines can be extended towards the vertical displacement axis to determine actual values. The "I"s at each data point represent the 95% confidence intervals for shear strain. The shear strain confidence intervals do not appear very well due to their narrowness. These data are compared to the noise distribution, which is the compilation of the histograms in Figure 2.9-2.11. Vertical dashed lines indicate the 95% confidence interval of vertical

noise signal displacement for no movement. These were calculated by applying kernel smoothing on the noise profile. Data with vertical displacements having a confidence interval that spans zero may be reasonably interpreted as being below the volumetric threshold shear strain. Alternatively, data points whose confidence intervals do not include zero are likely above threshold. Using the results shown in Figure 2.16, this interpretation leads to an estimate of volumetric threshold shear strain of approximately 0.03%.

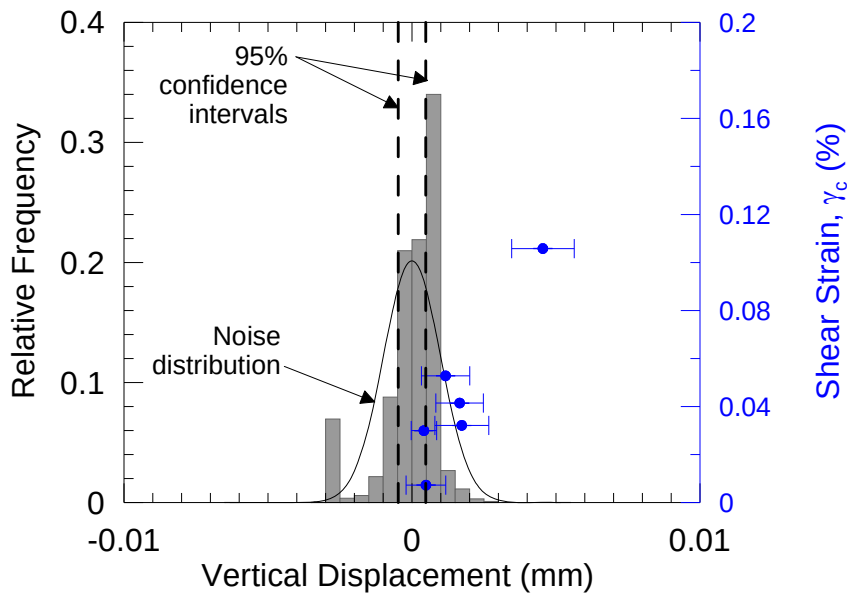

Figure 2.16 – Plot of sample test data with error bars against vertical noise signal distribution (no vertical movement).

Compiling test data for the Newhall#2 soil material results in Figure 2.17. Figure 2.17a, drawn with a linear vertical strain axis, illustrates the potential error associated with assigning a volumetric threshold shear strain based on simple visual interpretation of data plotted in this common form, which would result in a γ_{tv} value of approximately 0.1% in this case. Figure 2.17b, drawn with log axes, shows a linear trend in the vertical strain-shear strain plot. However, the data points at vertical strains below approximately 0.002% are not significantly different from zero, and hence fall below γ_{tv} per our definition.

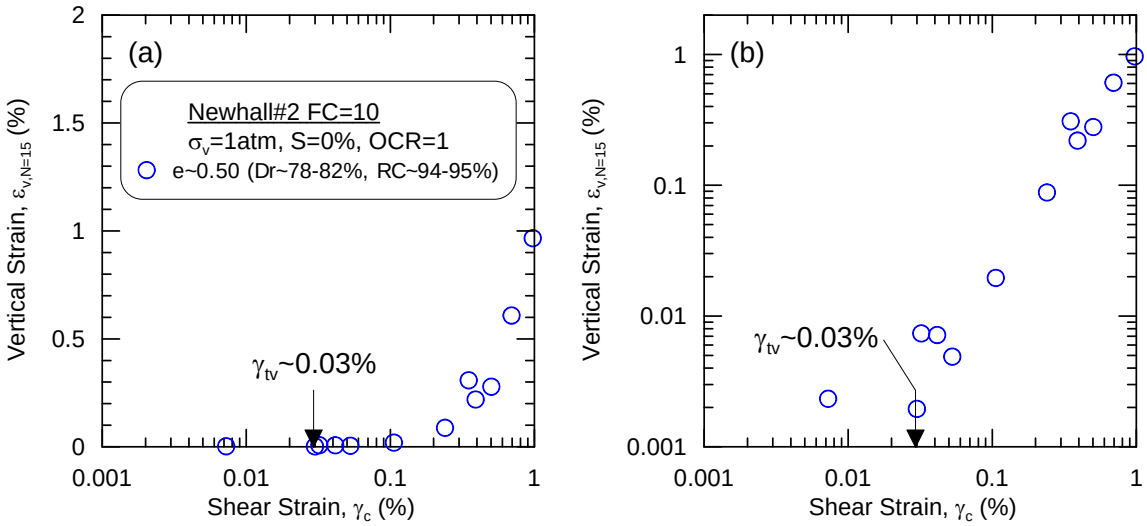

Figure 2.17 – Test results for soil material Newhall#2, FC=10%, D_R=80%, vertical stress=1atm, saturation=0%, and OCR=1. (a) Plot of vertical strain at N=15 cycles vs. shear strain (b) in log-log scale.

3. SEISMIC COMPRESSION BEHAVIOR OF A SAND-FINES MIXTURE INCLUDING OVERBURDEN AND STRESS HISTOY EFFECTS

3.1 SOIL TESTED

The base material was taken from the Newhall school Site B of Stewart et al. (2004) and will be called Newhall#2. The natural soil contains approximately 5% gravel and 14% fines. The clean sand was obtained by washing fines from the coarse fraction. Figure 3.1 shows the gradation curves for the clean sand and the fines portion. Mixtures of Newhall#2 clean sand and Newhall#2 fines were used for DC-SS testing.

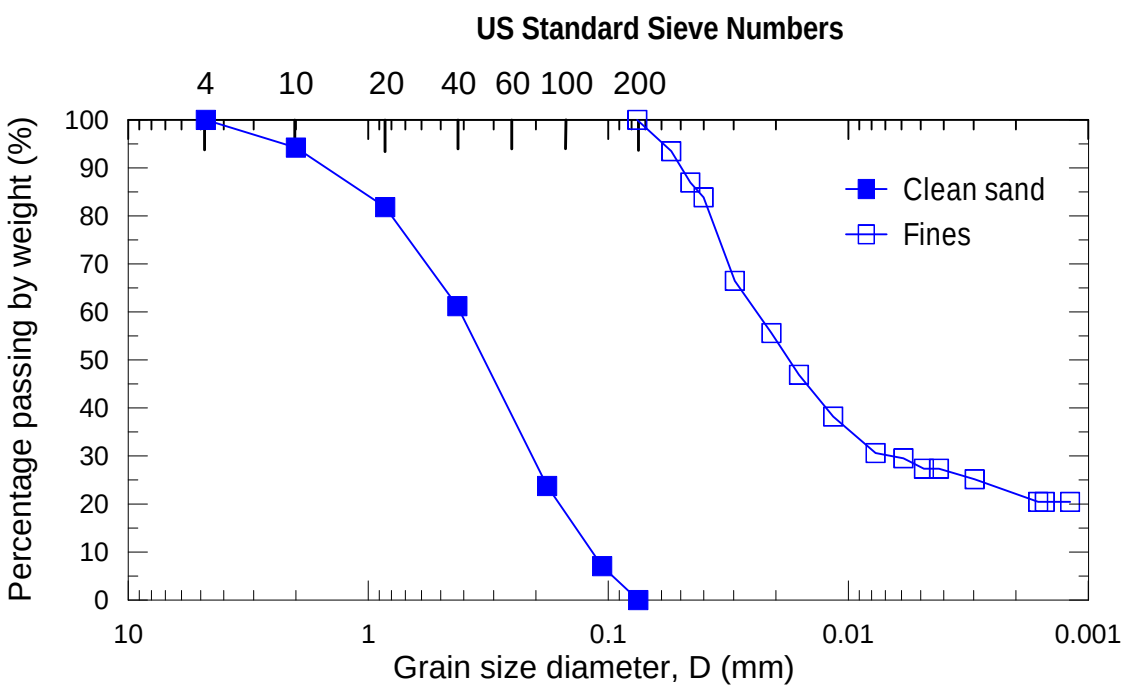

Figure 3.1 – Gradation curves for Newhall#2.

3.2 LABORATORY TEST EQUIPMENT AND PROTOCOLS

Laboratory testing was performed using the DC-SS device (Duku et al. 2007) with the same test procedures described in Duku et al. (2008). The testing program involves systematically testing Newhall#2 mixtures with FC=0, 10, and 50% for relative densities of 45, 60, and 80%. For each of these combinations, vertical stress and OCR are varied to evaluate their influence on volume change.

3.3 RESULTS OF CYCLIC SIMPLE SHEAR TESTS

3.3.1 FORM AND PARAMETERIZATION OF RESULTS

The test results are summarized using the form proposed by Duku et al. (2008), namely:

$$(\varepsilon_v)_{N=15} = a(\gamma_c - \gamma_{tv})^b \tag{3.1}$$

$$C_N = R\ln(N) + c \tag{3.2}$$

$$K_{\sigma,\varepsilon} = (\sigma_v / P_a)^{-0.29} \tag{3.3}$$

where:

N = number of cycles

$(\varepsilon_v)_{N=15}$ = volumetric strain after 15 cycles

γ_c = cyclic shear strain amplitude

γ_{tv} = volumetric threshold cyclic shear strain amplitude

C_N = volumetric strain ratio for N cycles

= $(\varepsilon_v)_N / (\varepsilon_v)_{N=15}$

a, b, R, c = regressed parameters

$K_{\sigma,\varepsilon}$ = vertical strain adjustment factor to account for overburden stress σ

= $\dfrac{a_\sigma}{a_{\sigma=1.0\ atm}}$

The following shows how parameters *b* and *R* are mathematically related through the model:

$$(\varepsilon_v)_N \,/\, (\varepsilon_v)_{N=15} = R\ln(N) + c$$

$$(\varepsilon_v)_N \,/\, (\varepsilon_v)_{N=15} = R\ln(N) + [1 - R\ln(15)]$$

$$(\varepsilon_v)_N \,/\, (\varepsilon_v)_{N=15} = 1 + R\ln(N/15)$$

$$(\varepsilon_v)_N \,/\, a(\gamma_c - \gamma_{tv})^b = 1 + R\ln(N/15)$$

$$a(\gamma_c - \gamma_{tv})^b = \frac{(\varepsilon_v)_N}{1 + R\ln(N/15)}$$

$$b\ln(\gamma_c - \gamma_{tv}) = \ln\left(\frac{(\varepsilon_v)_N}{a[1 + R\ln(N/15)]}\right)$$

$$b = \frac{\ln\left(\frac{(\varepsilon_v)_N}{a[1 + R\ln(N/15)]}\right)}{\ln(\gamma_c - \gamma_{tv})}$$

Parameters are obtained through nonlinear regression of test data.

3.3.2 EFFECT OF RELATIVE DENSITY AND FINES CONTENT

3.3.2.1 EFFECT OF RELATIVE DENSITY AND FINES CONTENT ON VERTICAL STRAIN

In the present investigation we use relative density as our metric of density. This is done because the fines considered are low-plasticity and dry. Hence, minimum and maximum void ratios (e_{min} and e_{max}) can be evaluated using ASTM procedures (ASTM D4253 and D4254). This enables a consistent evaluation of density effects across materials with different fines contents. However, we also recognize that the maximum density (corresponding to e_{min}) is difficult to achieve in soils with fines, and for this reason relative compaction (RC) is often a preferred metric of density for such materials. This is especially the case when the soil mixtures have moisture. Maximum dry densities for the soil mixtures with fines are indeed higher when evaluated using modified Proctor procedures than when using ASTM D4253. Further analysis of the data in terms of RC will be the subject of subsequent research.

Figure 3.2 summarizes the results of sample DC-SS testing for three Newhall#2 mixtures. These results indicate for a given relative density, increasing fines content increases the vertical strain after 15 cycles, which is consistent with the results of Whang et al. (2005). The plots also indicate for a given fines content, increasing relative density decreases vertical strain potential, which is consistent with previous research (Silver and Seed 1971, Youd 1972, Duku et al. 2008).

The data are parameterized and shown in Figure 3.3 and Figure 3.4. These figures are the results of simultaneously regressing parameters *a*, and *b*, with γ_{tv} set between 0.01-0.03% (Hsu and Vucetic 2004). Parameter *a* can be treated as the resultant vertical strain from a cyclic shear strain amplitude of approximately 1% and Figure 3.3a shows that as relative density increases, parameter *a* decreases. This data is compared to the clean sand model of Duku et al. (2008) and it becomes obvious that the Newhall#2 sand is a low outlier relative to the model (data falls near the mean – one standard deviation), which partially explains the conclusions by Whang et al. (2004) where soils with low-plasticity fines appeared to show lower vertical strains relative to sands, as the material used in their study is from the same site as Newhall#2. Figure 3.3b shows a strong increase of parameter *a* with fines content. As more test data is acquired and evaluated, the relationship can be more carefully explored.

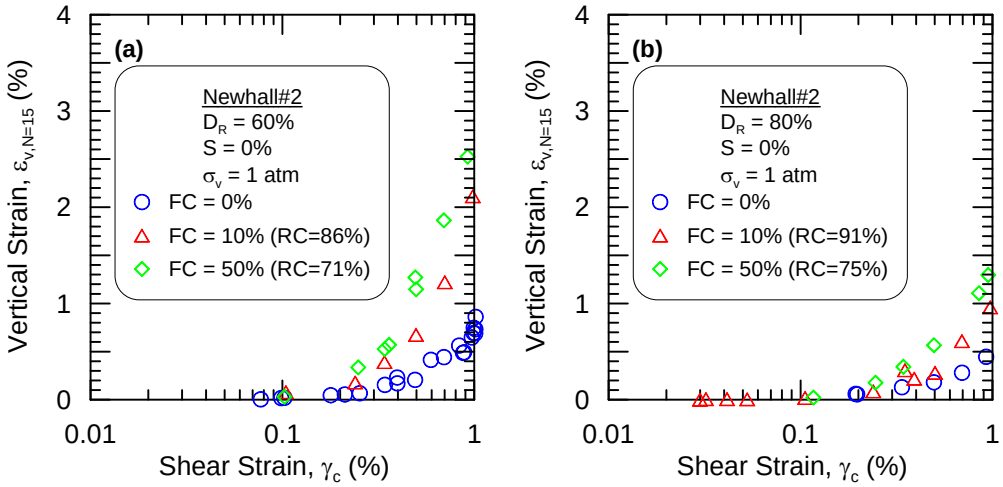

Figure 3.2 – Test results of varying fines content for (a) D_R=60% and (a) D_R=80%.

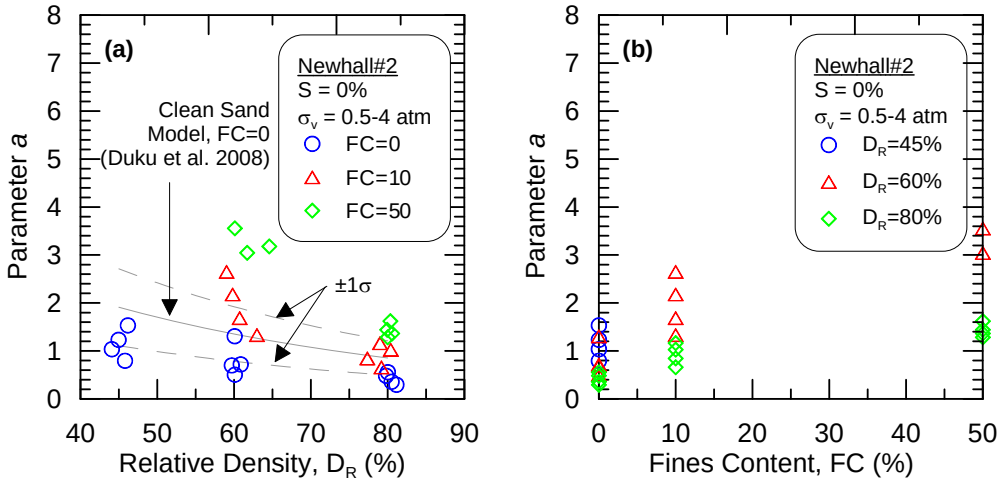

Figure 3.3 – Plot of parameter *a* against (a) relative density and (b) fines content.

Figure 3.4 shows little variation in parameter *b* against relative density and fines content. Parameter *b* as obtained from these tests is also similar to the Duku et al. (2008) model prediction.

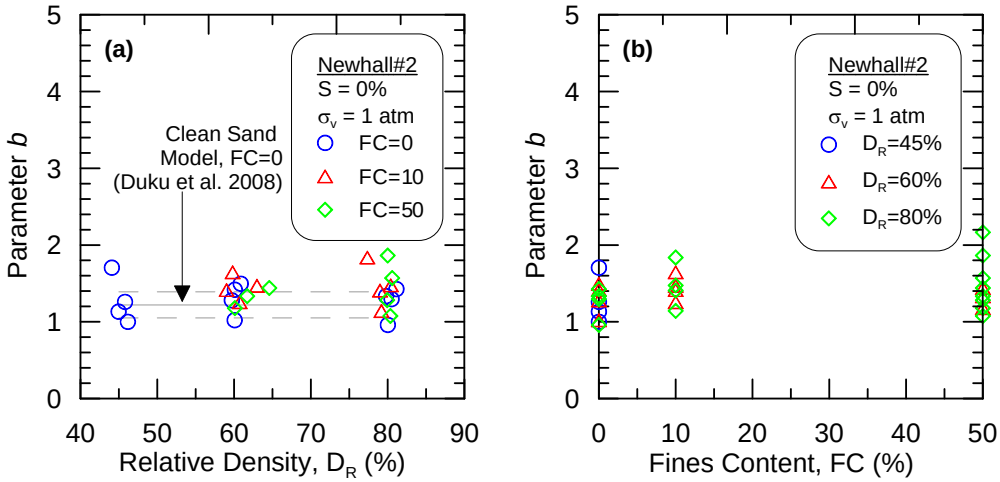

Figure 3.4 – Plot of parameter *b* against (a) relative density and (b) fines content.

The effects of fines content on vertical strain can be explained by research from Polito and Martin (2001) and Thevanayagam (1998).

Polito and Martin (2001) defined the parameter FC_L as the maximum amount of silt that can be contained in the void space between sand particles while maintaining a contiguous sand skeleton. For FC < FC_L, the addition of silt merely fills in inter-grain void space, thus decreasing void ratio. For FC > FC_L, sand grains float within a silt matrix, and increasing fines content increases the overall void ratio because intra-fines void ratios are relatively high. Hence, FC_L can be identified as the FC corresponding to lowest possible minimum void ratio, and is shown in Figure 3.5.

Thevanayagam (1998) postulated that a soil mixture can be viewed as being comprised of coarse-grained and fine-grained sub-matrices. For FC < FC_L, the finer-grain matrix does not actively participate in the transfer of contact frictional forces, or their contribution is secondary. It follows that the void ratio that controls soil behavior at FC < FC_L is the intergranular void ratio, e_s which is the void ratio of the sand fraction:

$$e_s = \frac{e + FC}{1 - FC} \tag{13}$$

At FC > FC_L the soil force chain is governed primarily by the contacts within the finer matrix and the coarser grains float in the finer-grain matrix. Consequently, the void ratio that is most controlling of soil behavior at FC > FC_L is the interfine void ratio, e_f:

$$e_f = \frac{e}{FC} \tag{14}$$

Using the above definitions, void ratio terms e_s and e_f are shown in Figure 3.5 along with the global void ratio corresponding to a relative density of 60% for Newhall#2 silty sand. Similar curves were obtained for other relative densities.

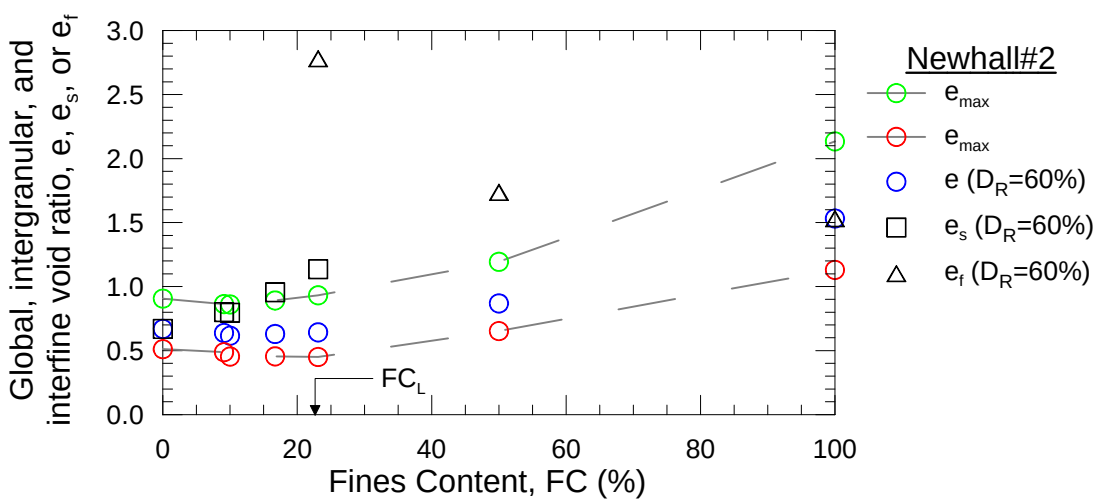

Figure 3.5 – Global (e), intergranular (e_s), and interfine (e_f) void ratio versus fines content for Newhall#2 silty sand.

The observed increase in seismic compression with increasing fines content below FC_L can be explained using the conceptual framework of Thevanayagam (1998) presented above. In particular, for FC < FC_L, the increase of intergranular void ratio (e_s) with FC explains the observed increase in $(\varepsilon_v)_{N=15}$ values, because e_s is the void ratio that controls the soil behavior for this range of FC. For FC > FC_L, the interfine void ratio, e_f, decreases with increasing fines content, which would suggest a reduction in $(\varepsilon_v)_{N=15}$

values with increasing fines content above FC_L. However, the opposite occurs, that is, $(\varepsilon_v)_{N=15}$ increases with fines content. This can be attributed to the fact that as FC increases the overall compressibility of the soil increases (lower bulk modulus), which in turn is likely related to the increase in global void ratio. Even though Figure 3.5 shows decreasing e_f with increasing fines content, the global void ratios above FC_L are generally larger than those below above FC_L, and the e_f above FC_L are larger than the e_s below the FC_L. Those high void ratios cause high compressibility (both static and cyclic), which more than overcomes the decreasing trend of e_f with FC.

3.3.2.2 EFFECT OF RELATIVE DENSITY AND FINES CONTENT ON NORMALIZED VERTICAL STRAIN

The effects of relative density and fines content on parameter R is shown in Figure 3.6. Figure 3.6a shows that parameter *R* does not vary significantly with relative density and is close to the clean sand model by Duku et al. (2008). However, Figure 3.6b shows a slight increase in parameter *R* as fines content increases. An increasing *R* would imply that the rate of cyclic settlement is higher and would be reflected in the *b* value. However, Figure 3.4b, does not show a significant increase if any at all. This trend cannot be confirmed as more data is needed to bridge the gap between FC=10 and FC=50.

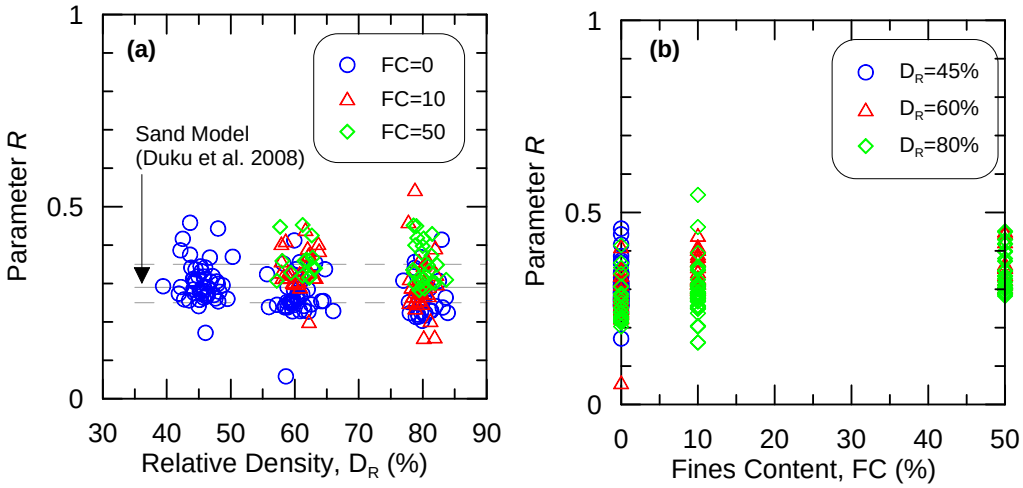

Figure 3.6 – Plot of parameter *R* against (a) relative density and (b) fines content.

Interestingly, when parameter *R* is plotted against cyclic shear strain amplitude, as in Figure 3.7, a minor trend appears where *R* generally increases as cyclic shear strain amplitude decreases. This trend appears to take effect at cyclic shear strains less than approximately 0.5%. However, in the small-strain range, the *R* values are relatively dispersed, which may be the result of measurement variability and the lack of a defined γ_{tv} for each dataset as vertical strains are approaching the noise magnitude. Another apparent trend is the general increase in *R* values as fines content increases across a range of cyclic shear strain amplitudes as shown in Figure 3.7b.

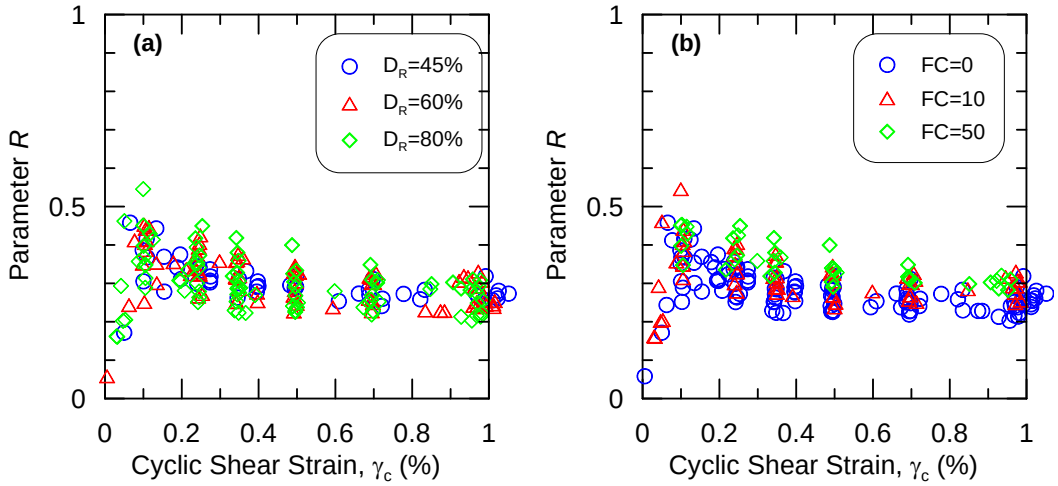

Figure 3.7 – Plot of parameter *R* against cyclic shear strain amplitude for (a) relative density and (b) fines content.

3.3.3 EFFECT OF OVERBURDEN

3.3.3.1 EFFECT OF OVERBURDEN ON VERTICAL STRAIN

Figure 3.8 summarizes the results of sample DC-SS testing for two Newhall#2 mixtures. These plots indicate for a given fines content, increasing the overburden decreases vertical strain potential.

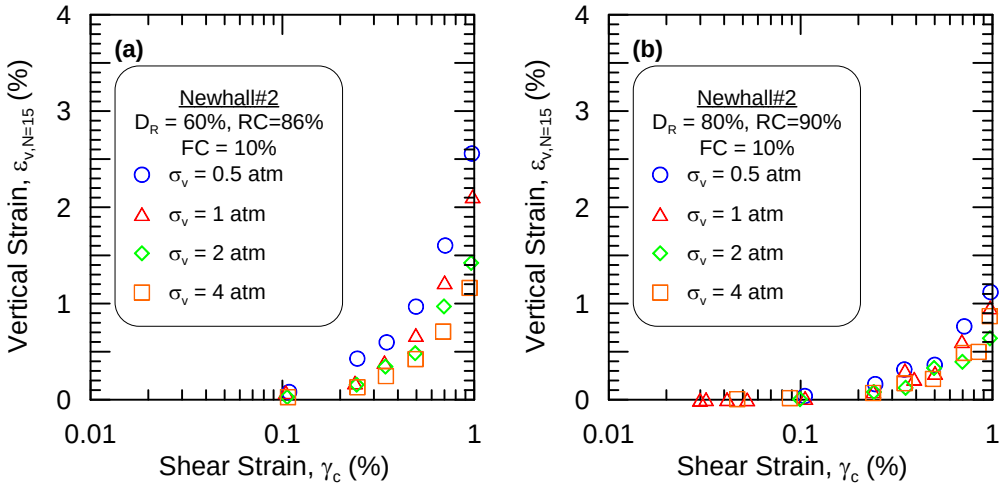

Figure 3.8 – Test results of varying overburden at FC=10% for (a) D_R=60% and (a) D_R=80%.

These results are parameterized and presented in Figure 3.9 and Figure 3.10. Figure 3.9 shows the normalized *a* value and surprisingly, it matches the sand model by Duku et al. (2008) quite well across the range of relative densities and fines content investigated ($K_{\sigma\varepsilon}$ is not dependent on either D_r or FC). Figure 3.10 shows a slight increase in parameter b as the vertical stress increases and the increase does not appear to be dependent on relative density or fines content.

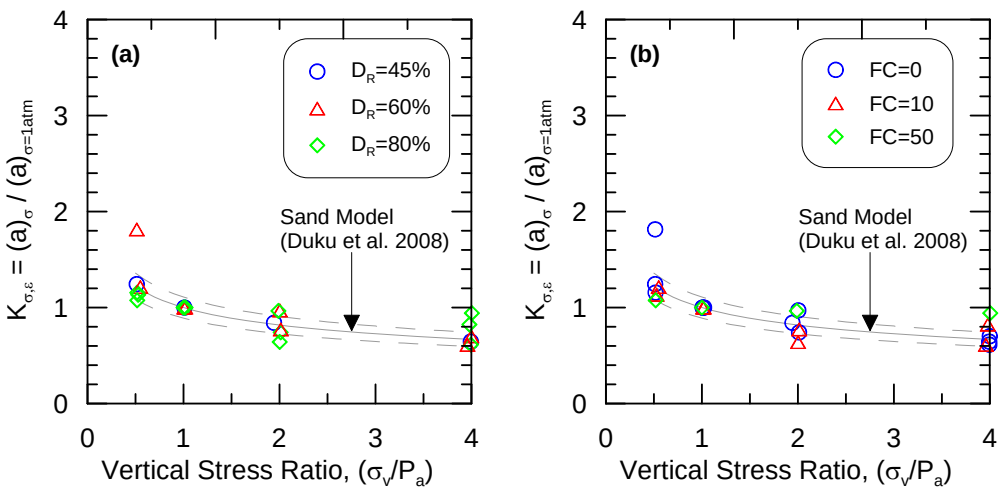

Figure 3.9 – Plot of parameter $K_{\sigma\varepsilon}$ against vertical stress ratio for (a) relative density and (b) fines content.

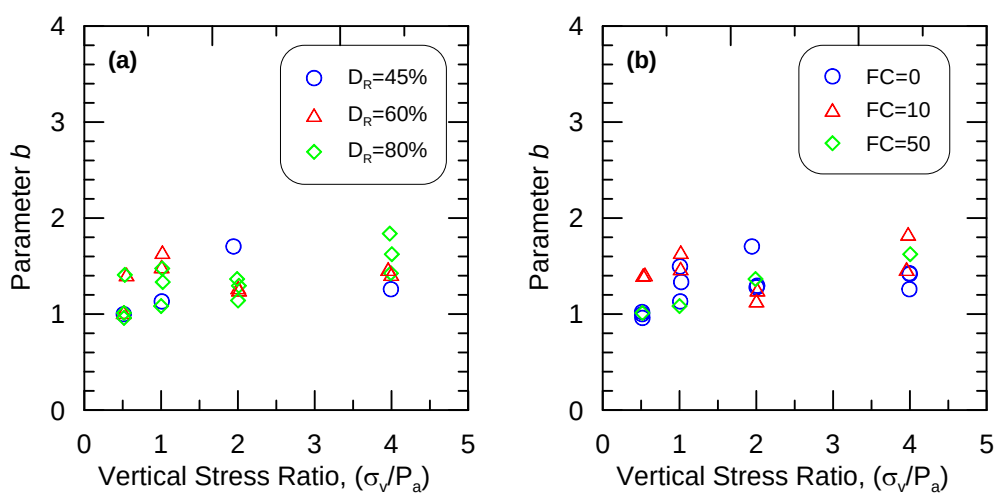

Figure 3.10 – Plot of parameter *b* against vertical stress ratio for (a) relative density and (b) fines content.

The observed dependence of seismic compression on vertical stress is in line with the findings of Duku et al. (2008) and deviates from previous findings by Silver and Seed (1971) and Youd (1972) for clean sands. As proposed by Duku et al. (2008), these findings can be interpreted through classical particle interaction concepts. By increasing the vertical stress on the soil sample, internal normal stresses between particles are also increased and as a result, an increase in interparticle contact areas. Due to increased interparticle contact areas, a larger fraction of the induced shear strains is used towards reducing the interparticle contact areas until plastic deformation (inter-particle slip) can occur. Since vertical strains from seismic compression are a result of plastic deformations, the increase in vertical stress should decrease vertical strain under a given level of cyclic shear deformation. This effect is also manifest by a reduction of bulk modulus with decreasing vertical stress.

3.3.3.2 EFFECT OF OVERBURDEN ON NORMALIZED VERTICAL STRAIN

Figure 3.11 plots *R* against vertical stress ratio. This plot does not show any significantly distinguishable pattern when viewed in terms of the vertical stress ratio.

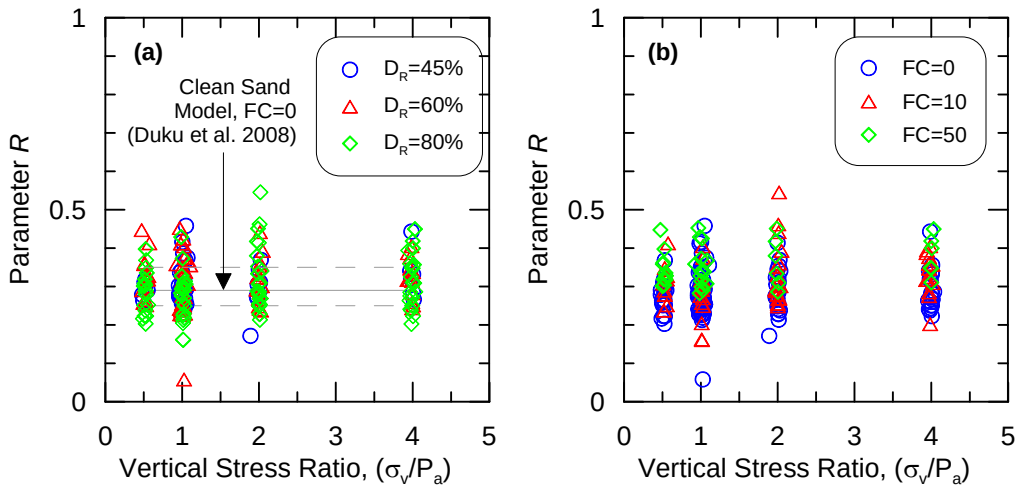

Figure 3.11 – Plot of parameter *R* against vertical stress ratio for (a) relative density and (b) fines content.

However, when parameter *R* is plotted against cyclic shear strain amplitude for varying vertical stress, a minor pattern emerges as shown in Figure 3.12. Figure 3.12a plots the data for FC=10 while Figure 3.12b plots the data for FC=50. Both plots show that for a given fines content an increasing vertical stress generally results in high *R* values. This is by and large consistent with the results shown in Figure 3.10 where the rate of displacement increases as overburden increases.

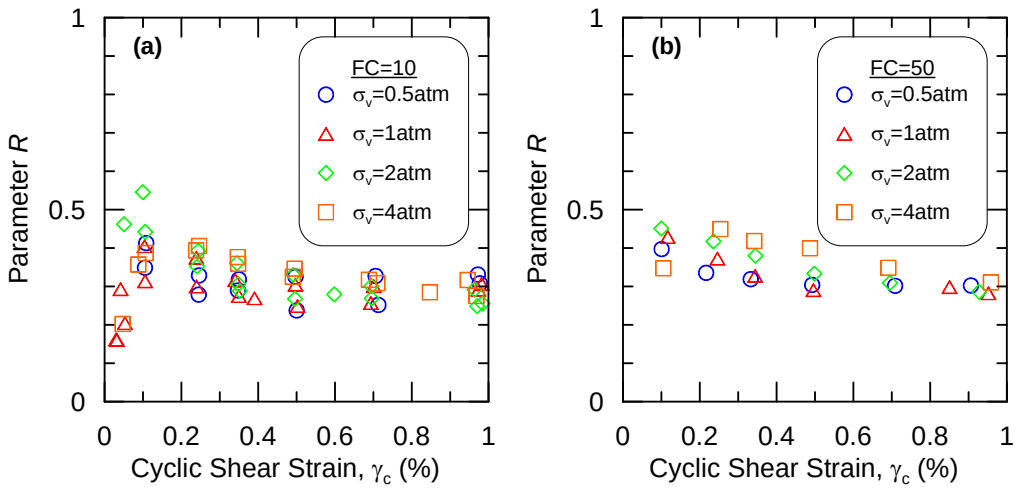

Figure 3.12 – Plot of parameter *R* against cyclic shear strain amplitude for (a) FC=10 and (b) FC=50.

3.3.4 EFFECT OF OCR

3.3.4.1 EFFECT OF OCR ON VERTICAL STRAIN

To investigate the effects of the overconsolidation ratio, OCR, on vertical strain, soil samples were loaded in the device to a target preconsolidation pressure and then unloaded to 1 atm. For example, to prepare a specimen for an OCR = 4, the soil sample would be vertically loaded in the device to 4 atm and allowed to sit long enough such that the settlement-time plot is effectively horizontal. The sample would then be unloaded to a vertical pressure of 1 atm and allowed to sit until the vertical LVDTs did not show a displacement change in the graphical user interface of the control software. Once this is done, a sample with an OCR = 4 is ready to be tested.

Figure 3.13 shows sample test data illustrating the effect of OCR. The plot shows that OCR significantly reduces vertical strains from seismic compression. Although some of the data are from very small cyclic shear strain amplitudes, their vertical displacement profiles either show no displacement or dilation before compression at later cycles. Example vertical strain profiles are show in Figure 3.14 to demonstrate suspected dilation behavior. This could be due to measurement noise and will be investigated in more detail in subsequent research.

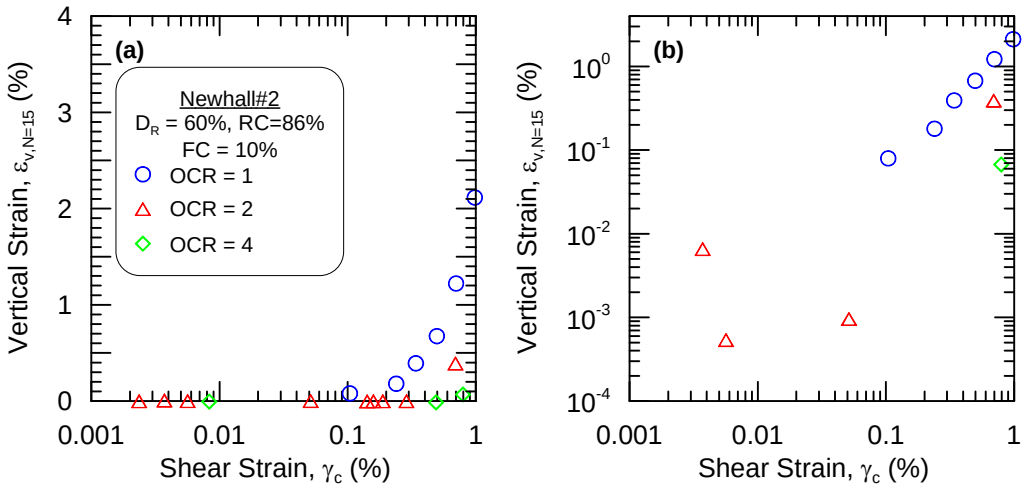

Figure 3.13 – (a) Test results of varying OCR at FC=10% (b) in log-log scale. Recall that data points below a vertical strain 2E-3% are not significantly different from zero per Section 2.3.4.

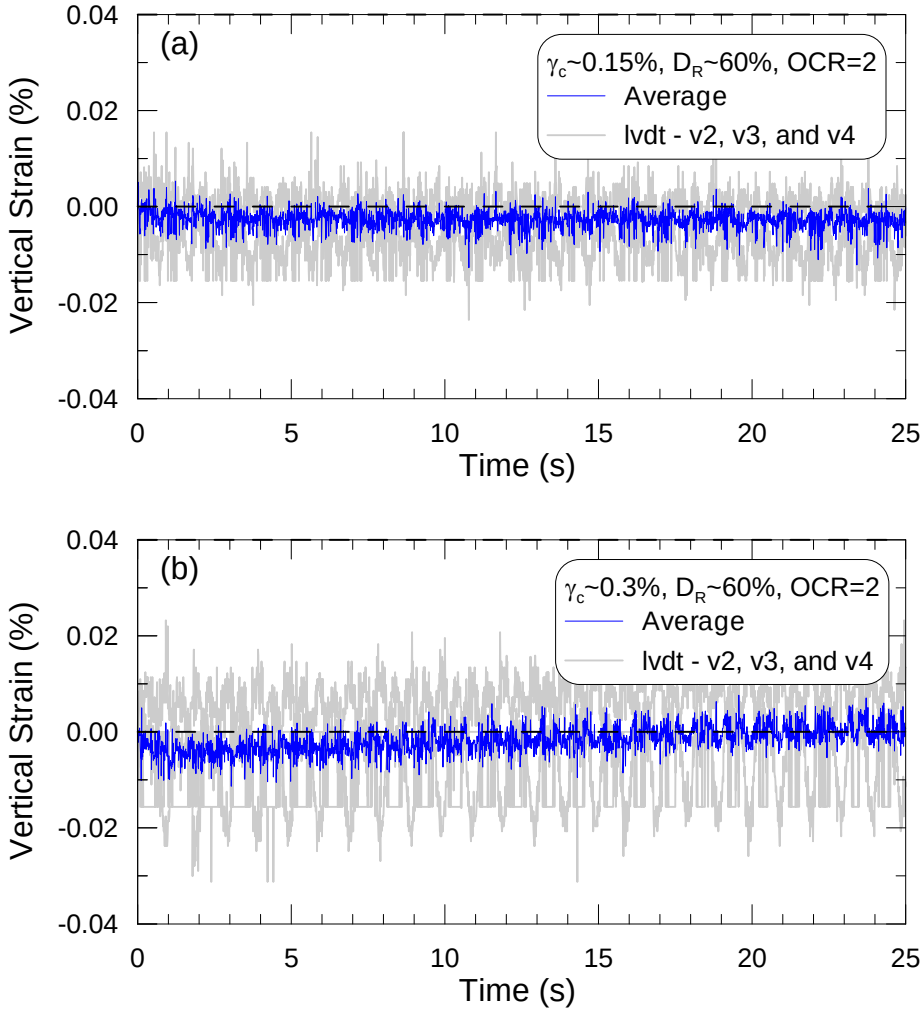

Figure 3.14 – Vertical strain profiles demonstrating dilation for (a) γ_c=0.15% and (b) γ_c=0.3%.

3.3.4.2 EFFECT OF OCR ON NORMALIZED VERTICAL STRAIN

Figure 3.15 plots *R* against cyclic shear strain amplitude for the limited amount of OCR related tests. The *R* values are extremely variable due to displacements very close to 0, but were not considered below the volumetric threshold shear strain because some of the sample data contain displacement profiles that show dilation and then compression.

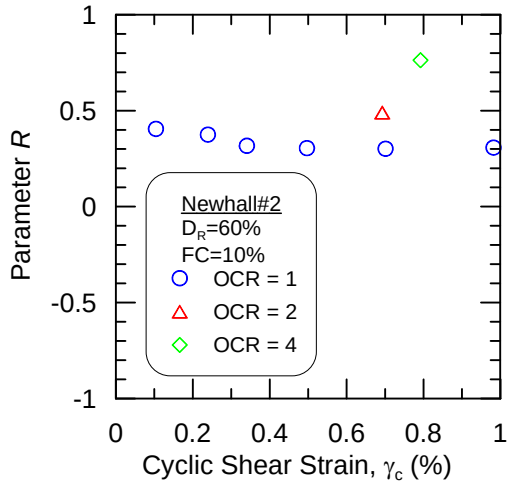

Figure 3.15 – Plot of parameter *R* against cyclic shear strain amplitude for FC=10.

3.3.5 EFFECT OF PRIOR CYCLIC LOADING

Figure 3.16 compares two data sets in evaluating the effects of prior cyclic loading. These effects were explored by taking already tested samples and re-applying another set of cyclic displacements. Therefore, one sample could produce multiple data points. Figure 3.16a compares repeated testing for soil samples with a relative density of 45%, a fines content of 0, and an overburden of 2 atm. Figure 3.16b compares repeated testing for soil samples with a relative density of 60%, a fines content of 0, and an overburden of 1 atm. Similar results were also found for other soil conditions. These are consistent with previous findings of soil materials that underwent prior cyclic shearing (Martin et al. 1975, Seed and Booker 1977).

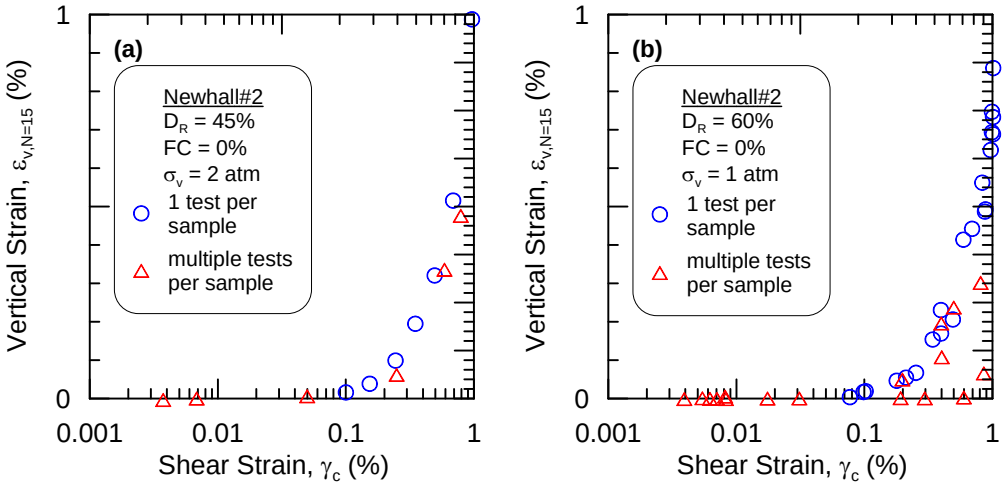

Figure 3.16 – Plot of data comparing shear history effects for a sample with (a) D_R=45%, FC=0, and σ_v=2atm and (b) D_R=60% , FC=0, and σ_v=1atm.

As shown in Figure 3.16, prior cyclic loading tends to decrease vertical strains. Generally, the larger the amplitude of the prior cyclic loading, the greater the decrease in vertical strain in subsequent cyclic loading. For example, a soil sample tested at γ_c = 0.1% and 0.5% would result in a larger vertical strain than a soil sample tested at γ_c = 0.1%, 0.2%, and 0.5%.

4. SUMMARY AND FUTURE RESEARCH NEEDS

This investigation has shown the largest volume change potential occurs in low-plasticity fine grained soils, which experience considerably more volume change than clean sands at a common relative density (or relative compaction). Test results also show vertical strain at fifteen shear strain cycles increases as relative density, overburden pressure, and OCR decrease, which is similar to previous test results on clean sands (Duku et al. 2008). Supplementary testing also showed soil samples that experienced prior cyclic loading tended to show a decrease in vertical strains when tested. Additionally, small-strain test results were analyzed using statistical techniques to formally quantify the uncertainty in data points given noise in the data acquisition system. These techniques allowed the development of a robust framework to extract volumetric threshold shear strain from test data taken from an appropriate apparatus.

While significant progress has been made, major questions remain such as the transition between large seismic compression potential (relative to clean sands) for low-plasticity fine grained soils and the relatively small seismic compression potential of higher plasticity fine grained soils (Whang et al. 2004, Duku et al. 2006). The research need lies in the fact that the available data is inadequate to define the transition. Other factors affect the seismic compression of fine-grained soils as well. For example, pseudo-overconsolidation brought on by volumetric creep (ageing) has been shown to significantly reduce the seismic compression potential of plastic fine grained soils, but to have no effect on non-plastic soils (Duku et al. 2006). A proper understanding of this factor in marginal plasticity materials will also be crucial to develop appropriate engineering models for seismic compression.

Hence, the research objective of future work can be stated as testing and VSMM development for marginal plasticity fine-grained soils as a function of soil composition (fines content, fines plasticity), compaction condition (relative compaction, saturation), and pseudo overconsolidation (representing ageing). The intent is to package the results as fines corrections to commonly used measures of soil penetration resistance (CPT tip resistance, SPT N value) to supplement the recently completed, similar model for clean sands. This form of the results will be very useful to working engineers.

REFERENCES

California Geological Survey (CGS). (2005). “Engineering geology and seismology for public schools and hospitals in California.” Rep. to Accompany California Geological Survey Note 48 Checklist, Sacramento, Calif., R. H. Sydnor, ed.

Duku, P. M., Stewart, J. P., and Whang, D. H. (2006). “Effect of postcompaction ageing on seismic compression of fine-grained soils.” Ground Modification and Seismic Mitigation, *Proceedings of the Sessions of GeoShanghai Conference*, A. Porbaha, S.-L. Shen, J. Wartman, and J.-C. Chai, eds., ASCE Geotechnical Special Publication No. 152, 411–416.

Duku, P.M., Stewart, J.P., Whang, D.H., and Venugopal, R. (2007), “Digitally controlled simple shear apparatus for dynamic soil testing,” *Geotechnical Testing Journal*, ASTM, 30 (5), 368-377.

Duku, P.M., Stewart, J.P., Whang, D.H., and Yee, E. (2008), “Volumetric strains of clean sands subject to cyclic loads,” *Journal of Geotechnical and Geoenvironmental Engineering*, ASCE, 134 (8), 1073-1085.

Härdle, W. (1990), Applied nonparametric regression, Econometric Society Monograph No.19, Cambridge University Press, New York. 333 p.

Hsu, C-C., and Vucetic, M. (2004), “Volumetric threshold shear strain for cyclic settlement”, *Journal of Geotechnical and Geoenvironmental Engineering*, ASCE, 130(1) 58-70.

Martin, G. R., Finn, W. D. L., and Seed, H. B. (1975), “Fundamentals of liquefaction under cyclic loading,” *Journal of Geotechnical Engineering Division*, ASCE, 101(GT5), 423-438.

Nadaraya, E.A. (1964), “On estimating regression”, *Theory of Probability and its Applications*, 9(1), 141-142.

Polito, C.P. and Martin, J.R. (2001), “Effects of nonplastic fines on the liquefaction resistance of sands”, *Journal of Geotechnical and Geoenvironmental Engineering*, ASCE, 127(5) 408-415.

Pyke, R., Seed, H.B., Chan, C.K. (1975), “Settlement of sands under multidirectional shaking,” *Journal of Geotechnical Engineering*, ASCE, 101 (4), 379-398.

Seed, H.B., and Silver, M.L. (1972), “Settlement of dry sands during earthquakes,” *Journal of Soil Mechanics and Foundations Division*, ASCE, 98(4), 381-397.

Seed, H.B. and Booker, J.R. (1977), "Stabilization of potentially liquefiable sand deposits," *Journal of Geotechnical Engineering Division*, ASCE, 103, no.7, pp. 757-768.

Seed, H.B., Idriss, I.M., and Arango, I. (1983), “Evaluation of liquefaction potential using field performance data,” *Journal of Geotechnical Engineering*, ASCE, 109(3), 458-482.

Seismic Safety Commission (SSC) (1995), “Northridge earthquake, turning loss to gain: Report to governor Pete Wilson in response to governor’s executive order W-78-94,” *SSC Report No. 95-1*, Seismic Safety Commission, State of California, Sacramento.

Silver, M.L., and Seed, H.B. (1971), “Volume changes in sands during cyclic loading,” *Journal of Soil Mechanics and Foundations Division*, ASCE, 97(9), 1171-1182.

Stewart J.P., Smith P.M., Whang D.H., and Bray J.D. (2004), “Seismic compression of two compacted earth fills shaken by the 1994 Northridge earthquake,” *Journal of Geotechnical and Geoenvironmental Engineering*, ASCE, 130(5), 461-476.

Thevanayagam, S. (1998), “Effect of fines and confining stress on undrained shear strength of silty sands,” *Journal of Geotechnical and Geoenvironmental Engineering*, ASCE, 124(6), 479-491.

Thibos, L.N. (2004), Fourier Analysis for Beginners, Bloomington, Indiana: Visual Sciences.

Tokimatsu, K. (2008), “Geotechnical problems in the 2007 niigata-ken chuetsu-oki earthquake,” *Proceedings of the conference of Geotechnical Earthquake Engineering and Soil Dynamics IV*, Sacramento, California, May 18-22, 2008, 1-30.

Tokimatsu, K., and Seed, H.B. (1987), “Evaluation of settlements in sand due to earthquake shaking,” *Journal of Geotechnical Engineering*, American Society of Civil Engineers, 113(8), 861-878.

Vucetic, M., (1994), "Cyclic threshold shear strains in soils," *Journal of Geotechnical Engineering*, ASCE, 120(12), 2208-2228.

Wartman, J., Rodriguez-Marek, A., Repetto, P.C., Keefer, D.K, Rondinel, E. Zegarra-Pellane, J., and Baures, D. (2003). “Ground failure” *Earthquake Spectra*, 19(S1), 35–56.

Watson, G.S. (1964), “Smooth regression analysis”, *Sankhya*, Series A, 26, 359-372.

Whang, D.H., Stewart, J.P., and Bray, J.D. (2004), “Effect of compaction conditions on the seismic compression of compacted fill soils,” *Geotechnical Testing Journal*, ASTM, 27 (4), 371-379.

Whang, D.H., Moyneur, M.S., Duku, P., and Stewart, J.P. (2005), "Seismic compression behavior of nonplastic silty sands," *Proceedings of the International Symposium on Advanced Experimental Unsaturated Soil Mechanics*, A. Tarantino, E. Romero, and Y.J. Cui (eds.), Trento, Italy, June 27-29, A.A. Balkema Publishers, pp 257-263.

Youd, T.L. (1972), "Compaction of sands by repeated shear straining," *Journal of Soil Mechanics and Foundations Division*, ASCE, 98(7), 709-725.